AD-A080 199 PURDUE UNIV HAMMOND IN DEPT OF MATHEMATICAL SCIENCES F/G 20/4
LATERAL BOUNDARY CONDITIONS FOR QUASISTEADY ATMOSPHERIC FLOWS.(U)
DEC 79 P GORDON N00014-78-C-0308
UNCLASSIFIED NL

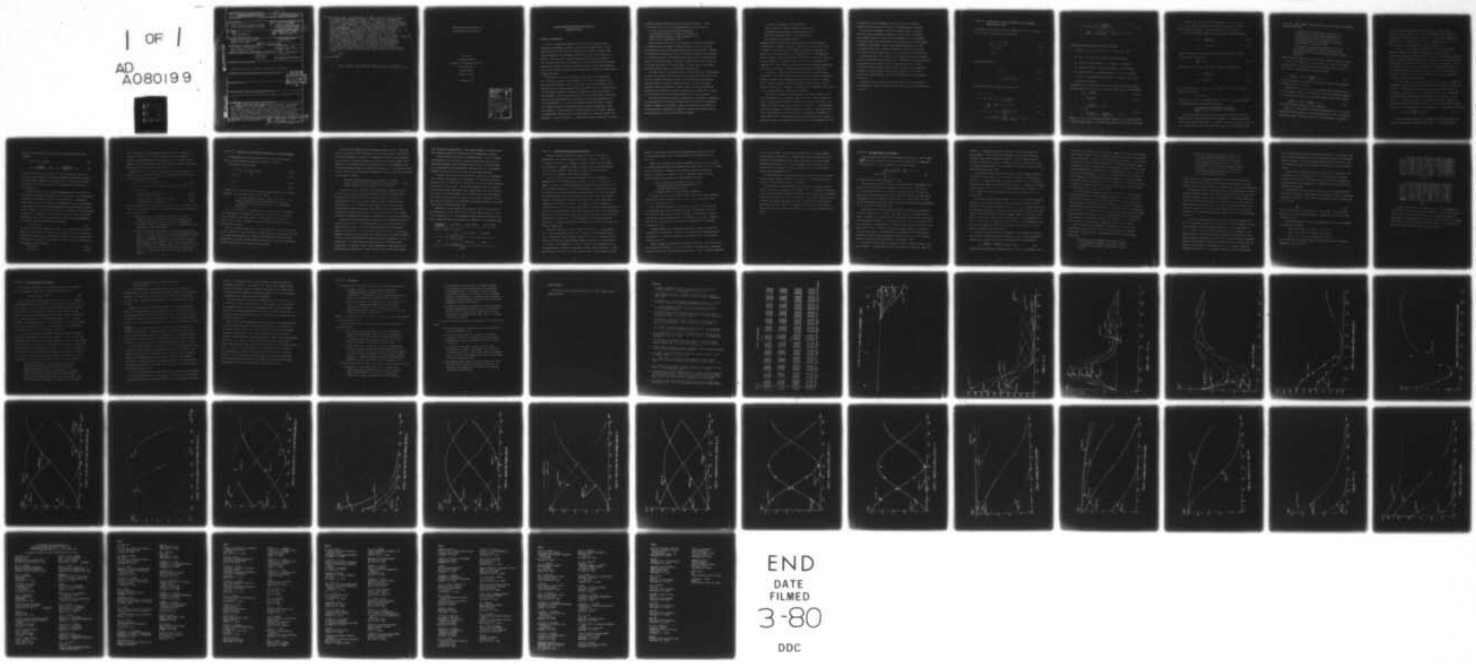

END
DATE FILMED
3-80
DDC

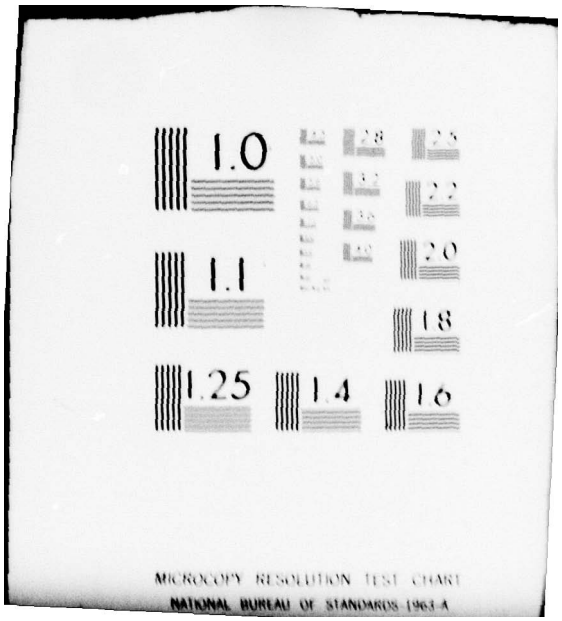
1.0
1.1
1.25
1.4
1.6
2.0
2.2
2.5
2.8
MICROCOPY RESOLUTION TEST CHART
NATIONAL BUREAU OF STANDARDS 1963-A

SECURITY CLASSIFICATION OF THIS PAGE (When Data Entered)

REPORT DOCUMENTATION PAGE

READ INSTRUCTIONS BEFORE COMPLETING FORM

1. REPORT NUMBER	2. GOVT ACCESSION NO.	3. RECIPIENT'S CATALOG NUMBER

4. TITLE (and Subtitle)
Lateral Boundary Conditions for Quasisteady Atmospheric Flows

5. TYPE OF REPORT & PERIOD COVERED
Progress Report
July 1 -- Dec. 31, 1979

6. PERFORMING ORG. REPORT NUMBER
1 Jul - 31 Dec 79

7. AUTHOR(s)
Paul Gordon

8. CONTRACT OR GRANT NUMBER(s)
N00014-78-C-0308
NR 061-254

9. PERFORMING ORGANIZATION NAME AND ADDRESS
Purdue University Calumet
Hammond, IN 46323

10. PROGRAM ELEMENT, PROJECT, TASK AREA & WORK UNIT NUMBERS
NR 061-254

11. CONTROLLING OFFICE NAME AND ADDRESS
U.S. Office of Naval Research
Fluid Dynamics Branch
800 N. Quincy St., Arlington, VA 22217

12. REPORT DATE
December 21, 1979

13. NUMBER OF PAGES
50

14. MONITORING AGENCY NAME & ADDRESS(if different from Controlling Office)

15. SECURITY CLASS. (of this report)
Unclassified

15a. DECLASSIFICATION/DOWNGRADING SCHEDULE

16. DISTRIBUTION STATEMENT (of this Report)

Approved for public release; distribution unlimited.

17. DISTRIBUTION STATEMENT (of the abstract entered in Block 20, if different from Report)

18. SUPPLEMENTARY NOTES

19. KEY WORDS (Continue on reverse side if necessary and identify by block number)

quasisteady models, free boundary conditions, atmospheric flows

20. ABSTRACT (Continue on reverse side if necessary and identify by block number)

The quasisteady model, derived by the author in an earlier paper [1], is extended to include lateral boundary conditions. The approach is to first assume a well-posed complete time-dependent problem, including boundary conditions; it is stressed that to each boundary condition there should be associated a precise physical assumption. It is then shown that the quasi-steady assumption can be applied consistently to both the partial differential equations and the boundary conditions, thereby → next page

DD FORM 1 JAN 73 1473 EDITION OF 1 NOV 65 IS OBSOLETE S/N 393867

SECURITY CLASSIFICATION OF THIS PAGE (When Data Entered)

cont.

obtaining a well-posed mathematical model with time scales suitable for large scale atmospheric flows. Three types of conditons are considered at the lateral boundaries: 1) outflow, 2) inflow (driven velocity is specified and is essentially independent of the internal flow, 3) inflow (passive) - inflow is created primarily by the inter flow configuration. The upper boundary conditions include the two derived in [1], the continuous and discontinuous boundary conditions, and a third condition, which is designed to allow the flow to propagate independently of the height of the region. Numerical solutions are obtained for various test cases, and convergence of the calculations is demonstrated. One sees that, although the calculations are reasonable, both from a mathematical and physical standpoint, the various calculations differ from each other very significantly, both qualitatively and quantitatively. It is suggested, therefore, that the process of specifying and evaluating boundary conditions will proceed more efficiently if more physical understanding is obtained in regard to relatively simple flows, such as a wave entering a stationary flow at a lateral boundary.

in an earlier paper

[1] P. Gordon, "Quasisteady Primitive Equations with Associated Upper Boundary Conditions", J. Math. Physics, V.20, April, 1979.

Lateral Boundary Conditions for Quasisteady Atmospheric Flows

Paul Gordon

Associate Professor

Department of Mathematical Sciences

Purdue University

Calumet Campus

Hammond, Indiana

December, 1979

Lateral Boundary Conditions for Quasisteady Atmospheric Flows

Section I: Introduction

In ref. [1] quasisteady equations were derived on the basis of scale assumptions approximately satisfied in large-scale atmospheric flow. Several upper boundary conditions were also derived, but the lateral boundaries were severely simplified. The underlying philosophy used in the above work was as follows: Assuming that the complete time-dependent problem is well-posed (this includes specification of boundary and initial conditions), derive internal equations and boundary conditions by employing clearly stated scale assumptions. In the present paper, an attempt is made to extend this approach to include lateral boundary conditions.

Difficulties with boundary conditions, particularly at free boundaries, arise in almost all areas of fluid dynamics. In the case of supersonic flow, the problems are generally simpler, since one can expect perturbations at such boundaries not to feed back upstream (see, for example, ref.[2]). Mathematically the hydrodynamic equations, representing a hyperbolic system, are reasonably well understood. This is particularly true for the one-dimensional case, although in two or more space dimensions, the existence and uniqueness theorems are not so well formulated [3]. It is in fact physical understanding that is lacking: It is perhaps impossible to specify physically "accurate" conditions at these free boundaries. This situation has so deteriorated that the scientist engaged in computational studies feels free in many instances to ignore the physics and mathematics. Chen [4] discusses "...computational boundary conditions, in contrast

to physical boundary conditions which are originally required..." Also, in his survey article [5, p.19], Belotserkovskii can write as follows:

> "...the basic principle underlying the statement of the conditions is that no substantial disturbances should penetrate through the "open" boundaries of the region into the computational region."

Various authors have written of the necessity of neither over-specifying nor under-specifying the number of boundary conditions [6,7,8]. In large scale atmospheric flow an additional stumbling block presents itself: Because of "simplifying" assumptions, such as the hydrostatic assumption, the equations are no longer hyperbolic. The question then arises anew as to even the proper number of boundary conditions. The paper of Oliger & Sundström [9] would seem to indicate that there is no "proper" number: A major result in this paper is that the hydrostatic model is not well-posed mathematically.

The above result has been quoted often in the last few years. Unfortunately, at least in the author's view, the result has at times been interpreted to mean that the researcher (since the equations are not well-posed anyway) can now experiment freely in terms of boundary conditions. In fact, Oliger and Sundström's work does produce the expected result: Having made quasisteady assumptions (the hydrostatic equation represents such an assumption), it should not be surprising that not all boundary conditions are still compatible.

This turn away from the physics is disconcerting. Historically, mathematics has been productive to the applied community when closely tied to the physical problem. Hadamard [10], who seems to have first introduced the concept of a well-posed problem, emphasized the importance of maintaining contact with the physical problem. In [10, p.32] he writes as follows:

"... But it is remarkable, on the other hand,
that a sure guide is found in physical interpretation:
An analytical problem always being correctly set, in
our use of the phrase, when it is the translation of
some mechanical or physical question..."

Hadamard's specific concern was different than ours (he was objecting to the mathematical assumption of analytic data), but his point is still valid. It appears to the author that in the area of computation the atmospheric physicist has relinquished much of his responsibility to the mathematician/numerical analyst. This is not intended to disparage the latter (if anything, the author would be so classified). Rather, the intent is to emphasize the importance of at least partially judging the results of numerical computations on the basis of the physical problem that one postulates is being solved.

For example, "reflective" behavior at a boundary may in some sense be undesirable, and its existence may in some sense be significant for diagnostic purposes. However, such a phenomenon remains at best a symptom. Since one does not define a physical problem by specifying "non-reflective", neither should one impose such a criterion on the mathematical formulation. And, needless to say, neither should it be imposed on the numerics.

One possible procedure for specifying outflow boundary conditions is to first assume physically a relatively simple form for the solution outside the region, and then specify boundary conditions associated with this flow. (one boundary condition proposed in this paper is of this form). In the atmospheric case such a procedure is difficult because so few "simple" solutions are known. This is particularly due to the fact that in an atmospheric environment even simple flows, such as a wave entering from a lateral boundary into a region of stationary flow, have extremely complicated solutions. Nevertheless, this lack

of knowledge is highly detrimental to both the process of specifying boundary conditions and to the evaluation of corresponding calculations.

The point to be emphasized is that the boundary conditions, however specified, must be interpreted physically in terms of what is inherently being assumed regarding the external flow configuration. This philosophy does differ greatly from that employed by most atmospheric scientists engaged in numerical calculations. Many of the techniques presently in use (see, for example, Orlanski [11], Perkey & Kreitzberg [12], and Kemp and Lilley [13]) share the common characteristics of not referring to the external flow.

Boundary conditions are discussed for the time-dependent case in Section II and for the quasisteady case in Section III. Calculations using these conditions are described in Section IV, V and VI: Section IV considers a problem involving internally generated flow, Section V considers a bell-shaped wave entering at a lateral boundary, and Section VI considers a "flat" wave entering at a lateral boundary. Section VII summarizes possible conclusions of the study.

An accuracy study, in terms of a decreased mesh size, was conducted for all calculations. Results of this study are shown for the bell-wave calculation in Section V.

Section II: Specification of Boundary Conditions for the Complete Time-Dependent Problem

The variables to be used are similar to those defined in ref. 1, except that the velocity components are now normalized:

$$\tilde{u} = (u - aw)/\sqrt{1+a^2} \tag{1.1}$$

$$\tilde{w} = (w + au)/\sqrt{1+a^2} \tag{1.2}$$

$$\pi = \frac{p}{\bar{p}}^{(\gamma-1)/\gamma} \tag{1.3}$$

$$\theta = \frac{1}{\bar{\rho}}\frac{p}{\bar{p}}^{1/\gamma} \tag{1.4}$$

Using the transformation

$$\tau = t \tag{2.1}$$

$$\eta = x/L \tag{2.2}$$

$$\zeta = \frac{z - f_1(t,x)}{f_2(t,x) - f_1(t,x)} \tag{2.3}$$

The hydrodynamic equations take the following form:

$$\theta_\tau = -r\theta_\zeta - \frac{u}{L}\theta_\eta \tag{3.1}$$

$$\tilde{u}_\tau = -G_1 = -r\tilde{u}_\zeta - \frac{u}{L}\tilde{u}_\eta - \frac{c_s^2}{(\gamma-1)\pi L\sqrt{1+a^2}}\pi_\eta$$

$$+ \frac{ag}{\sqrt{1+a^2}} - \frac{\tilde{w}}{1+a^2}(a_\tau + ra_\zeta + \frac{u}{L}a_\eta). \tag{3.2}$$

$$\pi_\tau = -G_2 = -r\pi_\zeta - \frac{u}{L}\pi_\eta - \frac{(\gamma-1)\pi}{L\sqrt{1+a^2}}(\tilde{u}_\eta + a\tilde{w}_\eta) \tag{3.3}$$

$$- (\gamma-1)\pi\zeta_z\sqrt{1+a^2}\,w_\zeta - \frac{(\gamma-1)\pi}{\sqrt{1+a^2}}\left(\frac{w}{L\sqrt{1+a^2}}a_\eta - \tilde{u}\zeta_z a_\zeta\right)$$

$$\tilde{w}_\tau = -G_3 = -r\tilde{w}_\zeta - \frac{u}{L}\tilde{w}_\eta - \frac{c_s^2\zeta_z\sqrt{1+a^2}}{(\gamma-1)\pi}\pi_\zeta \qquad (3.4)$$

$$- \frac{g}{\sqrt{1+a^2}} - \frac{ac_s^2}{(\gamma-1)\pi L\sqrt{1+a^2}}\pi_\eta + \frac{\tilde{u}}{1+a^2}(a_\tau + ra_\zeta + \frac{u}{L}a_\eta)$$

The various parameters defined above are as follows:

$a = \zeta_x/\zeta_z$, $r = \zeta_t + w\zeta_z + u\zeta_x$, $\gamma = 1 + R/c_v$, $c_s^2 = \gamma RT$,

$\bar{p} = p/P_0$, $\bar{T} = T/T_0$, f_1 = position of the lower boundary,

f_2 = position of upper boundary, ρ = density, T = temperature,

w = vertical velocity, u = horizontal velocity, R = gas constant,

c_v = specific heat, x = horizontal distance, z = vertical distance,

t = time, g = acceleration due to gravity, p = pressure = ρRT, ρ_0 and

T_0 are reference values.

The equations for the floating top and for the continuous and discontinuous boundary conditions [1: eqs. 10, 15, 21] take respectively the following form:

$$(f_2)_\tau = \tilde{w}\sqrt{1+a^2} \qquad (4.1)$$

$$\pi_\tau = \frac{(\gamma-1)\pi}{c_s}\tilde{w} \qquad (4.2)$$

$$\pi_\tau = \begin{cases} \dfrac{(\gamma-1)\pi}{c_s}\tilde{w}_\tau & : \quad \tilde{w} \le 0 \\ \dfrac{(\gamma-1)\pi}{c_s}\tilde{w}_\tau - \dfrac{(\gamma-1)\pi g}{c_s^2}(f_2)_\tau & : \quad \tilde{w} > 0 \end{cases} \qquad (4.3)$$

Remark: In ref. 1 the discontinuous boundary condition was written incorrectly in that the scale factor $(1 + a^2)^{-\frac{1}{2}}$ was omitted from the first term on the right.

A solution is to be obtained in the region $0 \leq \zeta \leq 1$, $0 \leq \eta \leq 1$, $0 \leq \tau \leq \tau_{end}$. Before considering the boundary conditions for eq.(3) at the four spatial boundaries, a general condition will be discussed.

A simplified one-dimensional model consists of the following equations:

$$u_t = - \frac{c_s^2}{(\gamma-1)\pi} \pi_x \tag{5.1}$$

$$\pi_t = - (\gamma-1)\pi u_x \tag{5.2}$$

Assuming a steady wave, moving with velocity c_w, one "watches" the wave front approach by the equation,

$$\frac{dx}{dt} = -c_w \quad . \tag{5.3}$$

Substituting eq.(5.3), eqs. (5.1) and (5.2) take the following form:

$$u_t = \frac{c_s^2}{(\gamma-1)\pi c_w} \pi_t , \tag{5.4}$$

$$\pi_t = \frac{(\gamma-1)\pi}{c_w} u_t \quad . \tag{5.5}$$

In the case that $c_w = c_s$ (that is, a sound wave), eqs. (5.4) and (5.5) both become the following:

$$u_t = \frac{c_s}{(\gamma-1)\pi} \pi_t \quad . \tag{5.6}$$

Eq.(5.6) has been used as a boundary condition in earlier work [14,15], where the following physical interpretation was given:

> At a boundary eq.(5.6) models a sound wave, moving into an infinite region of undisturbed flow.

Eq.(5.6) will be used in this paper as a boundary conditon. An obvious objection would be that the problem of most interest in atmospheric situations will not be sound-wave dominated. It is tempting, therefore, to use c_w in eq.(5.3) as a "fudge-factor" by which one could obtain various forms of either eq.(5.4)

or eq.(5.5). This approach has been avoided, and in this regard the following points are pertinent:

i) The philosophy of this paper, as discussed in the introduction, is that the boundary conditions must make an assumption in terms of the external flow. It is incorrect, therefore, to calculate c_w "adaptively" from conditions of the internal flow.

ii) If specific two-dimensional steady-state solutions to atmospheric problems were known, then perhaps these solutions could be used to derive more appropriate boundary conditions.

Specific boundary conditions at the four spatial boundaries will now be given.

A) $\zeta = 0$ is assumed to be a solid boundary. An appropriate boundary condition is $\tilde{w} = 0$. One can then obtain θ and $\tilde{u}$ from eqs.(3.1) and (3.2), while π can be calculated from the following equation:

$$\frac{c_s}{(\gamma-1)\pi}\pi_\tau - \tilde{w}_\tau = -\left(\frac{c_s}{(\gamma-1)\pi}G_2 - G_3\right) \qquad (7.1)$$

Eq. (7.1) represents the linearized characteristic variable which propagates information from $\zeta > 0$ to $\zeta = 0$.

B) Because of eq. (4.1), $\zeta = 1$ is a streamline and consequently one and only one boundary condition is required here. The three differential equations to be used are eqs.(3.1) and (3.2), and the following characteristic equation:

$$\frac{c_s}{(\gamma-1)\pi}\pi_\tau + \tilde{w}_\tau = -\left(\frac{c_s}{(\gamma-1)\pi}G_2 + G_3\right) . \qquad (7.2)$$

Three upper boundary conditions will be considered.

1) Eq.(4.2): This equation was derived mathematically in ref [1] as the continuous boundary condition. The interpretation given by (6) is not entirely valid here because the derivative in eq.(4.2) is with respect to τ and not t.

Thus, with this boundary condition, the floating top pushes a line of constant pressure (namely $\zeta = 1$) into the "undisturbed" region and then superimposes the change dictated by eq.(4.2). In essence, the characteristic variable of eq. (7.1) remains constant as it propagates from $\zeta > 1$ to $\zeta = 1$; this, of course, ignores hydrostatic changes far above $\zeta = 1$.

2) Eq.(4.3): This equation was derived in [1] as the discontinuous boundary condition. The physical interpretation is that the flow at $\zeta = 1$ behaves as a weak compression wave moving into a region of relatively undisturbed flow. However, the assumption now is that the wave acts at the moving boundary with respect to the undisturbed hydrostatic pressure at that position. That is, the change dictated by eq.(4.2) is imposed on the undisturbed region above $\zeta = 1$; the second term on the right in eq.(4.3), for $\tilde{w} > 0$, accounts for the hydrostatic change in pressure. Interpretation (6) would seem, therefore, to be valid for this boundary condition.

3) Both eqs.(4.2) and (4.3) assume that the flow above $\zeta = 1$ is relatively undisturbed. There are situations where this physical assumption is clearly not justified. One such example would be that of an incoming lateral wave, with the assumption that the wave is also entering above the region of computation. A possible physical assumption for this flow would be as follows: The flow above $\zeta = 1$ propagates laterally in a one-dimensional fashion, without being significantly affected by the flow below $\zeta = 1$. This is modeled mathematically by eq.(5.6), with interpretation (6). Transforming to τ, one obtains the following:

$$\pi_\tau + \zeta_t \pi_\zeta = \frac{(\gamma-1)\pi}{c_s} (\tilde{u}_\tau + \zeta_t \tilde{u}_\zeta) \ . \qquad (8)$$

C) At the lateral boundaries, three boundary conditions are required for inflow and one otherwise (assuming subsonic flow). At a non-inflow point

eq.(3.1) can be used along with the following linearized characteristic equations:

$$\tilde{au}_\tau - \tilde{w}_\tau = -(aG_1 - G_3) \tag{9}$$

$$\tilde{u}_\tau \pm \frac{c_s\sqrt{1+a^2}}{(\gamma-1)\pi}\pi_\tau + a\tilde{w}_\tau = -(G_1 \pm \frac{c_s\sqrt{1+a^2}}{(\gamma-1)\pi}G_2 + aG_3) \tag{10}$$

In eq.(10), the plus sign is used at $\eta = 1$ and the negative sign at $\eta = 0$. As at the other boundaries, the additional boundary conditions must reflect a physical assumption regarding the outside flow. At the non-inflow points it was decided to use either eq.(8), with the same physical interpretation, or the condition $u = 0$.

At inflow points, eq.(10) - with the appropriate sign - can be used, but three additional boundary conditions need to be specified. This is particularly troublesome for θ because of the fact that perturbations in θ propagate so slowly, namely at the flow velocity: the computational times to be considered in this paper are far less than the approximately 14 hours required to traverse 500 km. at 10m/sec. It was decided, therefore, to assume that θ is not perturbed by outside flow. Physically, this would imply that θ is constant on incoming streamlines, but it is not so clear how best to interpret this mathematically. The following equation was eventually settled upon:

$$\theta_\tau + r\,\theta_\zeta = 0. \tag{11}$$

In order to determine the remaining conditions, it is necessary to distinguish between "forced" inflow and "passive" inflow. Forced inflow, which represents physically an external flow being impressed on the region, can be modeled simply: Either velocity or pressure is specified. For purposes of the present paper, it was decided to specify velocity:

$$\tilde{u} = h_1(t,z) \tag{12.1}$$

$$\tilde{w} = h_2(t,z) \tag{12.2}$$

(Eqs. (10) and (11), then, essentially determine θ and π). However, the second case, where flow is in effect pulled into the region because of internally produced gradients, is more complicated. One possible physical assumption would be that the wave enters as a sound wave normal to the surface. Mathematically, this translates to eqs.(8) and $w = 0$.

Summarizing, eq.(3) at interior points and the following equations at boundary points are assumed to define a well-posed mathematical formulation of a well-defined physical problem:

i) $\zeta = 0$: $\tilde{w} = 0$, (3.1), (3.2), (7.1). (13.1)

ii) $\zeta = 1$: (3.1), (3.2), (7.2) and one of [(4.2),(4.3),(8)]. (13.2)

iii) $\eta = 0$ or 1:

a) non-inflow: (3.1),(9),(10), $u = 0$ (13.3)

or, (3.1),(9),(10),(8). (13.4)

b) forced inflow: (10),(11),(12.1),(12.2) (13.5)

c) passive inflow: (10),(11),(8), $w = 0$ (13.6)

The above formulation does not consider the corner points: ($\eta = 0,1;\zeta = 0,1$). Several severe problems, which have been consistently ignored in the literature, arise at these points:

i) There are two sets of equations, corresponding to the two boundaries, that can be used. Generally, one attempts to use those relationships which are forcing the flow configuration. For example, an algebraic boundary condition, because of continuity requirements, is considered forcing.

ii) Since the linearized characteristic equations are in general not valid, it may become necessary to use a partial differential equation directly. For example, if the flow is being forced at $\eta = 0$, $\zeta = 0$, then it is reasonable to impose eqs.(12.1), and (12.2), with $h_2 \equiv 0$, and to impose θ, say with eq.(11), but one expects to calculate π from the internal flow. However, neither eqs.(3.2) and (7.1), from the $\zeta = 0$ set, nor eqs.(10) and (11) from the $\eta = 0$ set, can be applied. In this case one might be forced to use eq.(3.3), $\pi_\tau = -G_2$, directly.

Section III: Specification of Boundary Conditions for the Quasisteady Model

The quasisteady equations are obtained from eq.(3) by assuming that π and $\tilde{w}$ are in quasisteady equilibrium with respect to θ and $\tilde{u}$[1].

The following equations result:

$$\left.\begin{aligned} \theta_\tau &= -r\theta_\zeta - \frac{u}{L}\theta_\eta\,, \\ \tilde{u}_\tau &= -G_1, \end{aligned}\right\} \quad \text{unchanged} \qquad (14.1),\ (14.2)$$

$$G_2 = 0, \qquad (14.3)$$

$$G_3 = 0. \qquad (14.4)$$

It remains now to study the effect of the quasisteady assumption on the boundary conditions. The underlying principle is as follows:

> If a boundary equation involves π_τ or $\tilde{w}_\tau$, and if the equation involves flow conditions internal to the region of computation, then the equation will be put in quasisteady equilibrium. (15)

At $\zeta = 0$ the situation is relatively simple. $\tilde{w} = 0$ and eqs.(3.1) and (3.2) remain unaffected by the quasisteady assumption. According to (15), however, eq.(7.1) becomes a quasisteady equation. This means that the right side of eq.(7.1) is set to zero. Because of eqs.(14.3) and (14.4), then, eq.(7.1) is deleted from the system.

At $\zeta = 1$ a similar analysis holds: Eqs.(3.1) and (3.2) are still valid, while eq.(7.2) is deleted. On the other hand, the upper boundary conditions are unaffected by the quasisteady assumption: Although involving quasisteady variables, these equations do not require internal conditions of the flow; in fact, the "derivation" of these equations related to external flow conditions.

At the lateral boundaries a more complicated situation exists. First note that eqs.(14.3) and (14.4) were derived only at internal points of the flow and need not in principal be imposed at the boundaries. However, if these equations are not used at the lateral boundaries, the resulting solution may exhibit steep gradients. Such gradients will be inconsistent with the scale assumptions upon which the quasisteady equations are based [1, assumption 2]. (This perhaps relates to the discussion in the introduction regarding the results of Oliger and Sundström). One concludes as follows:

> The basic quasisteady assumption [1, assumption 2] requires that eqs.(14.3) and (14.4) be applied at all points of the lateral boundaries except possible at the corner points. (16)

As noted in ref. [1], the effect of the quasisteady equations, eqs.(14.3) and (14.4), is to remove internal time dependence from the variables π and $\tilde{w}$. Boundary conditions must account for the time-dependence: $\tilde{w} = 0$ at $\zeta = 0$ accomplishes this for $\tilde{w}$ and the upper boundary condition provides the time dependence for π. It is important to note that eqs.(4.2) and (4.3) provide time dependence relative to the upper flow, while eq.(8) also relates to the external lateral flow; therefore, if eq.(8) is used at the top it is necessary to consider the possibility of incurring inconsistencies at the lateral boundaries.

Consider first non-inflow points and assume the upper boundary condition is either eq.(4.2) or (4.3). If the lateral equation set is given by (13.3), one would use eqs.(3.1) and $u = 0$ for the quasisteady model, and if the lateral equation set is given by (13.4), one would use eqs.(3.1) and (8). If the upper boundary condition is given by eq.(8), the situation remains the same for equation set (13.3), but an inconsistency can arise with respect to equation set (13.4). clearly near $\zeta = 1$, eq.(8) cannot be used to calculate u "laterally" and π "vertically". In this case, since it seems reasonable to assume that $\tilde{u}$ can be obtained from the internal flow, eq.(3.2) has been used directly (this assumes

that the required time-dependence at the lateral boundary is provided by the upper boundary condition in conjunction with the quasisteady equations).

At forced inflow the situation is reasonably clear. Eq.(10) is deleted from equation set (13.5) because it involves internal time derivatives of quasisteady variables, and the algebraic equation (12.2) is deleted because it is inconsistent with the quasisteady equation, eq.(14.3). The remaining equations, eqs.(11) and (12.2), are used with the quasisteady model.

At passive inflow points eq.(11) can still be applied in the quasisteady case. As above, eqs.(10) and $w = 0$ are deleted. The remaining equation of equation set (13.6), namely eq.(8), can be used if the upper boundary condition is given by eq.(4.2) or (4.3). If the upper boundary condition is given by eq.(8), then the same inconsistency, as discussed above, can arise if eq.(8) is also used at the lateral boundary. This situation has not yet been resolved. One possible solution might be to again use eq.(3.2) for $\tilde{u}$ (perhaps it is in some sense the "residue" of the quasisteady limit process relative to eq.(10)). Further study is required for this case.

Summarizing, the quasisteady model consists of eqs.(14.3) and (14.4) at all points and eqs. (14.1) and (14.2) at all points except possibly $\eta = 0$ or 1. $\tilde{w} = 0$ is imposed at $\zeta = 0$. The additional feasible boundary conditions to be used in conjunction with these equations are summarized in the following table:

Top Boundary Condition	non-inflow	forced inflow	passive inflow
(4.2) or (4.3)	(3.1), $u = 0$ or (3.1), (8)	(11), (12.1)	(11), (8)
(8)	(3.1), $u = 0$ or (3.1), (3.2)	(11), (12.1)	(11), ?

TABLE 1

Section IV: Internally Generated Outflow and Inflow

The basic numerical scheme can be found in ref.[1] and will not be repeated here. All boundary conditions are solved implicitly (that is, at the forward time step). For example, at a lateral boundary eq. (3.2) would be differenced as, $\frac{1}{\Delta t}\left(u_{i,j}^{n+1} - u_{i,j}^{n}\right) = -(G_1)_{i,j}^{n+1}$, where one-sided differences would be used as required. Since eqs.(14.3) and (14.4) are also solved implicitly, the iteration problem becomes complicated.

The initial data used for the test problems in ref.[1] consisted of a stationary flow with a lateral pressure gradient in a region of height h and length L. Because the lateral boundaries were assumed to be solid walls (u = 0 was the boundary condition), the flow thereby generated proceeded to reflect from the boundaries. In the present study, the right boundary will be a free boundary. The lateral boundary conditions must therefore allow the flow to move through and then, as it turns out, to move back into the region. These results will be compared with the following test case: The region is tripled to length 3L, initial data in $0 \leq x \leq L$ is as above, data for the additional region is stationary flow with no pressure gradient. This latter problem is solved with the quasisteady model and u = 0 at the lateral boundaries. During a reasonably long time period, during which the results at x = L are independent of the boundary conditions imposed at x = 3L, the results obtained with the large region can be compared with the free boundary case.

The initial flow field, for the region $0 \leq x \leq 480$ km. = L, is as shown in fig. 1 (this is reproduced from ref.[1]). $\tilde{w}$ and $\tilde{u}$ are zero throughout at time zero. Overpressure, with no pressure gradient in $L < x < 3L$, is shown in fig. 2. For this test case the continuous upper boundary condition, eq.(4.2) was used at $\zeta = 1$, and u = 0 was imposed at $\eta = 0$ and 1. Figure 3 shows pressure at z = 0 for various times. Initially a "secondary" pressure front forms near x = L (this can be seen at t = 1600), but by 2400 sec. this front is moving toward the right

boundary. This pressure distribution is accompanied by a reverse flow; this can be seen from figures 4 and 5, which display the $\tilde{u}$ distribution at $\zeta = 0$ and $\zeta = 1$.

Ideally, one would now like to specify boundary conditions at $x = L$ so that the solution thereby obtained would reproduce the above flow in $0 \leq x \leq L$. It seems fairly clear that for a problem of this complexity such a goal cannot be attained. Nevertheless, because the flow is internally generated, one can expect to obtain the following with proper boundary conditions:

a) The flow should be qualitatively correct (in this case outflow and reverse flow should occur in a generally appropriate time scale).

b) Quantitatively, the results should be comparable.

If inflow occurs, it will be passive inflow. Thus, the following boundary conditions are used (see table 1): At $x = \eta = 0$, $u = 0$ and eq.(3.1), and at $x/L = \eta = 1$, eqs.(8) and (11).

This solution was run until time 4000 sec. In ref.[1] it was shown that the oscillation time for this boundary condition was approximately 1600 sec. This implies a wave velocity of $L/1600 \approx 300 \frac{\text{m.}}{\text{sec.}}$, or about 6400 sec. would be required for the wave to travel from L to 3L and back. It was felt, therefore, that for this time period the results should be independent of the boundary condition at $x = 3L$.

Boundary condition (8) is intended to represent a situation in which the external flow is undisturbed. Clearly, for this problem this assumption is not valid near $x = L$. However, it perhaps is satisfied for the flow sufficiently distant from $x = L$.

Figure 6 compares the pressure distribution at two times. The solid dots are the results using eq.(8) at $x = L$. At time 800 sec. the comparison is very good, while at time 4000 sec. some discrepancy can be seen. Figure 7 shows the comparison

in u at the top surface. The effect of eq.(8) seems to be to delay somewhat the development of reverse flow. The author judges this comparison to be good: In addition to maintaining the time scale of the problem, the results remain reasonable quantitatively also: It might perhaps also be noted that this is considered to be a difficult test case, particularly because of the combined inflow-outflow configuration at x = L.

It seems reasonable to suppose that even better agreement could be obtained by appropriately "tuning" the factor c_s in eq.(8). For the reasons discussed in Section II, such a procedure was not attempted.

A calculation was also made with eq.(3.2) replacing the boundary condition eq.(8); that is, $\tilde{u}$ is calculated at the boundary x = L. The physical significance is not clear, particularly because this condition seems to make no direct assumption regarding the external flow. It is interesting to note therefore that the results, not shown, are sensible numerically, but show little agreement with the results obtained with the large region. For example, at time 4000 sec., the pressure distribution has oscillated back essentially to the distribution existing at time 800 sec.

Section V: Bell-Wave Input at Left Boundary

For this case the initial flow is stationary and hydrostatic: $\tilde{u} = \tilde{w} = 0$, $\frac{\partial \pi}{\partial z} = -\frac{(\gamma-1)g}{c_o^2 \theta}$, $\theta(0,x,z) = \theta(0,0,z)$ and $\theta(0,0,z)$ is as in the test case of Section IV [1, eq.(22.8)]. At $x = 0$ $\tilde{u}$ is specified as a function of time:

$$\tilde{u}(\tau,0,\zeta) = \begin{cases} 16\, u_{max}\left(\frac{\tau}{c_1}\right)^2\left(1 - \frac{\tau}{c_1}\right)^2 : & 0 < \tau < c_1 \\ 0: & t > c_1. \end{cases} \qquad (17)$$

$\tilde{u}$ thereby achieves a maximum of u_{max} at $\tau = c_1/2$.

The first calculation uses eq.(8) at the upper boundary. Consequently, from table 1, eq.(11) and (12.1) were imposed at $\eta = 0$ and eqs.(3.1) and (3.2) at $\eta = 1$ (note that inflow at $\eta = 1$ does not occur for this case). The values of u_{max} and c_1 were taken respectively as 2.5 and 3200. Figure 8 shows the velocity distribution at the top surface for various times. At time 4800 sec. this wave has left the region, and the flow, except for a small perturbation of approximately 4%, has returned to a stationary flow.

This residual flow, which apparently proceeds to oscillate back through the region with values $|\tilde{u}| < .1$ and $|\tilde{w}| < .005$, does not seem to be numerical error. Rather, it appears to be related to the difficulty noted in Section II of achieving a true steady-state solution. This difficulty is due to the slow time scale of θ. At time 6000 sec., the variation of θ from its values at time zero is still on the order of 10^{-4}; this is sufficient to maintain pressure gradients to account for the values noted above. To partially check this statement, the calculation was repeated with θ held constant throughout the region ($\theta \equiv \theta_o = 1.05$). The "residual" values of velocity in this case were $|\tilde{u}| < .001$ and $|\tilde{w}| < .0001$.

The shape of the wave form, as a function of time, is shown in Figure 9. The curve labeled x = 0 represents eq.(17) for the conditions given above. The curve

labeled x = L represents the velocity curve as it exits the region at the upper boundary. Since the region was initially in equilibrium, one expects the wave to move through relatively unchanged. The curve shown for eq.(8) indicates that this is the case. In addition, there is no damping of the wave. The exiting velocity curve at z = 0 is similar to that shown in Figure 9, except that the maximum value is 2.288.

This problem was next solved with the other two upper boundary conditions. From table 1, eqs.(11) and (12.1) are used at $\eta = 0$ and eqs.(3.1) and (8) are used at $\eta = 1$. Again, the shape of the curve is maintained well. The vertical distribution is somewhat more pronounced for this case. For example, the maximum outflow velocity at $\zeta = 0$ is $\tilde{u} = 2.151$, while the maximum value of $\tilde{u}$ at $\zeta = 1$ is 2.505. Figure (10) shows the horizontal velocity distribution at $\zeta = 0$ for various times.

For the discontinuous boundary condition, eq.(4.3), the results are markedly different. Since a small pressure gradient is maintained at the top surface, horizontal velocity falls off rapidly at the top. In fact, as noted in Figure (11), the wave does not reach the far boundary, but instead decays rapidly. This would indicate that a large amount of energy is being dissipated to the outside upper region. Velocity at $\zeta = 0$ does build up more completely: The maximum value of $\tilde{u}$ at ($\zeta = 0$, $\eta = \frac{1}{2}$) is 1.5 and occurs at time 2800 sec., while the maximum value at the right boundary ($\zeta = 0, \eta = 1$) is .1 and occurs at time 3800 sec. By time 4800 sec.,a complete reverse flow exists.

It was also thought of interest to combine the upper boundary conditions. Eqs.(8) and (4.3) together make little sense, since each contains a hydrostatic pressure term. However, eqs.(8) and (4.2) produce the following equation:

$$\pi_\tau = \frac{(\gamma-1)\pi}{c_s} \tilde{w}_\tau + \frac{(\gamma-1)\pi}{c_s} (\tilde{u}_\tau + \zeta_\tau \tilde{u}_\zeta) - \zeta_\tau \pi_\zeta \quad . \tag{18}$$

Although the precise physical interpretation of eq.(18) is not completely clear,

the idea is to combine both a vertical effect, namely eq.(4.2), with the horizontal effect given by eq.(8). Figure 12 shows results of the calculation using eq.(18) at the top and eqs.(3.1) and (3.2) at the right lateral boundary. It is seen that the wave form is much like that obtained with the individual equations (compare with Figures 8 and 9). However, there is an important distinction in that eq.(18) produces some damping of the wave form: The maximum value of u at $\eta = 1$ is 2.36 and occurs at approximately $t = 3100$ sec. This damping appears to be totally an upper boundary effect, unrelated to the lateral boundaries: Note that the wave is already depressed by time 2400 sec. Also, comparison at an earlier time, before the wave has propagated into the region, shows no appreciable difference between the three cases eq.(8), eq.(4.2), and eq.(18).

The three boundary conditions, eqs.(4.2),(4.3), and (8), differ in another important characteristic, namely dependence on height. Eq.(8) was "designed" to minimize this dependence: The physical assumption that the flow is also being imposed above $\zeta = 1$ indicates that the wave profile at $\zeta = 1$ should be relatively unaffected by the height of the lower region. This was verified by a calculation with a height of 5 km. instead of 10 km. The other two boundary condition, however, assume undisturbed flow above $\zeta = 1$ and consequently should be height dependent. This dependence is reflected in the form of the equations: Eqs.(4.2) and (4.3) involve vertical velocity, which is a quantity very sensitive to height.

Figure 13 compares two calculations, with heights of 10 km. and 5 km. respectively, both using eq.(4.2) at the top and the same lateral boundary conditions as discussed earlier. Two features of the flow are particularly interesting:

1) The smaller region propagates the wave more slowly. This is perhaps as expected, since vertical velocity is smaller and consequently pressure builds up more slowly.

2) There is a damping effect related to height. The 5 km. case produced a maximum outlet velocity of 1.89 m/sec., while for the 10 km. case the maximum outlet velocity was shown to be 2.505. Perhaps for this combination of wave input and boundary condition the height of 10 km. is some kind of "magic number": At this height the wave propagates across the field in a relatively unperturbed manner.

Clearly, there is a significant mathematical relationship between the wave input, the height of the region, and the upper boundary condition. At the present time what one requires here is a physical explanation of this relationship.

As discussed in ref.[1], the floating top is an important part of the model. Figure 14 displays the motion of the top for the case with eq.(8) as the upper boundary condition. In general this motion parallels the velocity profile, as can be seen by comparing with Figure 8. This was also true for the cases of boundary conditions (4.2) and (18). The maximum perturbation for each of the three cases (using eq.(8),(4.2), and (18) respectively) was 87.6 m., 81.75m., and 87.4m. For the discontinuous boundary condition, eq.(4.3), the top boundary rose 241.5 m.

As in the test case of Section IV, the lateral boundary conditions were tested by increasing the length of the region. The region was doubled in length, with the boundary conditions formerly imposed at $x = L$ now being imposed at $x = 2L$. Figures 15 and 16 show typical results of this investigation. This particular data is from the case with upper boundary condition (18) and right lateral conditions given by eqs.(3.1) and (3.2). The solid lines are the results obtained with the doubled length, while the solid dots are the results with the original length of 480km. The agreement at $\zeta = 1$ is very good, while some discrepancy builds up a $\zeta = 0$. The author concludes that these calculations

give strong assurance that the lateral boundary conditions, in conjunction with the given upper boundary condition, are consistently modeling the hypothesized physical situation. In this case the hypothesized physical situation is that of an external flow which is undisturbed "sufficiently far" from the region of interest.

Accuracy of the computations, relative to mesh size, is considered to be an important part of a numerical study. Of the three classes of problems discussed in this paper, the bell-wave problem of this section displayed the steepest gradients and consequently also displayed the greatest difficulty in establishing convergence.

As discussed in [1], one should at least be able to demonstrate that the solutions of a numerical algorithm behave as though they are part of a convergent sequence of calculations. For a first order method the following criterion was derived in [1]:

$$\frac{\Delta 2}{\Delta 1} \leq .5, \tag{19}$$

where $\Delta 1 = f^*(\tau,\eta,\zeta,h) - f^*(\tau,\eta,\zeta,\frac{h}{2})$, $\Delta 2 = f^*(\tau,\eta,\zeta,\frac{h}{2}) - f^*(\tau,\eta,\zeta,\frac{h}{4})$, and $f^*(\tau,\eta,\zeta,h)$ is the numerical approximation, obtained with step-size h, to the variable $f(\tau,\eta,\zeta)$.

For the problem using eq.(8) at the upper boundary, the following sequence of calculations was made:

run 1: Δx = 20 km., $\Delta z \sim$ 1.25 km., Δt = 40 sec.,

run 2: Δx = 10 km., $\Delta z \sim$ .625 km., Δt = 20 sec.,

run 3: Δx = 5 km., $\Delta z \sim$ .3125 km., Δt = 10 sec.

At time 1600 sec., the following tables display typical results for various quantities in the flow field:

	$\tilde{u}(\tau,\frac{1}{2},1)$	$\tilde{w}(\tau,\frac{1}{2},1)$	$\Delta f_2(\tau,0)$	$P(\tau,\frac{1}{2},0)$	$\theta(\tau,\frac{1}{2},\frac{1}{2})$
run 1	1.4634	.0747	46.75	1034.448	.0000064
run 2	1.4683	.0739	46.42	1034.938	.0000071
run 3	1.4694	.0734	46.20	1035.078	.0000075
$\Delta 1$	-.0049	.0008	.33	-.490	-.0000007
$\Delta 2$	-.0011	.0005	.22	-.140	-.0000004
$\Delta 2/\Delta 1$	.224	.625	.667	.286	.57

Table 2

	$\tilde{u}(\tau,1,0)$	$\tilde{u}(\tau,1,1)$	$P(\tau,0,0)$	$P(\tau,0,1)$	$\tilde{w}(\tau,0,1)$
run 1	.0054	.0041	1038.503	268.697	.0049
run 2	-.0002	-.0007	1038.915	268.730	.0013
run 3	-.0011	-.0012	1039.014	268.757	.0001
$\Delta 1$	.0056	.0048	-.412	-.043	.0036
$\Delta 2$	.0009	.0005	-.099	-.027	.0012
$\Delta 2/\Delta 1$	.161	.104	.240	.63	.333

Table 3

In general, criterion (19) is satisfied very well. Δf_2 represents the actual motion of the top surface and θ represents the deviation of θ from its initial value: In both these cases there is some question regarding the significance of the digits shown in the table. Note also that $P(\tau,0,1)$ changes little from its initial value (namely 269.039), while $P(\tau,0,0)$ changes much more significantly (from its initial value of 1029.792).

Section VI: Flat Wave Input at Left Boundary

The problem is precisely as that discussed in Section V, except that eq.(17), the input function for $\tilde{u}$, is replaced by the following:

$$\tilde{u}(\tau,0,\zeta) = u_{max}(1-e^{-c_1\tau^2}) \quad . \tag{20}$$

For the sample calculation u_{max} was again 2.5 and $c_1 = 10^{-6}$. Using the upper boundary condition eq.(8) and the lateral boundary conditions (at $\eta = 1$) eqs.(3.1) and (3.2), one obtains the solution depicted in Figures 17 and 18. The solution at the top surface is as expected: the velocity builds up, according to eq.(20), and propagates across the field. However, the solution at $\zeta = 0$ was not expected, in that the maximum velocity at $\eta = 0$ did not propagate in the expected time scale. (By time 6000 sec., the profile changes little from that at time 4000 sec.). The "discrepancy" is approximately the same as that seen earlier in the bell-wave calculation.

It is clear, from simple conservation of mass considerations, that the solution as shown cannot be a steady-state solution. It is also clear, from calculations with reduced mesh size, that numerical error cannot account for the unexpected form of the solution. One next needs to ask whether the calculation satisfies the original time-dependent problem. This is difficult to judge, but if the answer is no, then presumably the quasisteady equations are not valid.

As noted in ref[1], the quasisteady equations do introduce errors into the solution. In the present problem this error can be seen clearly at $\eta = 0$:

> The velocity input at $\eta = 0$ would, with eqs.(3), produce a pressure increase with a significant non-hydrostatic vertical variation (at least in the short term). One expects, over the long term, that the vertically propagating "fast" characteristics will dissipate the "non-hydrostatic" variation. The quasisteady equations, on the other hand, ignore the short-term time-development, and thereby inherently assume

that any steep gradients at $\eta = 0$ are not important in the long term.

It is not thought that the above error would account for the results shown in Figures 17 and 18. One expects the error introduced by the quasisteady equations to be manifested, not in the final flow profiles, but in the short-term time scale. Relative to the time-scale of the problem, this error should be small.

Referring to eq.(3.2), one sees that the π_η term is the most important factor in the propagation of $\tilde{u}$. The coefficient of this term involves only θ. A calculation with θ constant should, then, remove much of the vertical variation, but would not affect the quasisteady assumptions. Such a calculation was made, with $\theta \equiv 1.05$. In this case the variation in sound speed was even more pronounced: $\frac{(c_s)_{bottom}}{(c_s)_{top}} = 1.22$. The velocity profiles are much like those of Figure 17, except slightly retarded. However, there is no significant variation between the top and bottom horizontal velocity. Furthermore, this calculation achieves a steady-state: By time 4400 sec., the variation in the position of the top surface is 1.3m (from $\eta = 0$ to $\eta = 1$), and the maximum value of $|\tilde{w}|$ is .0001.

A more careful analysis of the original calculation (with variable θ) shows that the solution, although not in steady-state, is very slowly varying. For example, at time 6000 sec. the variation in the position of the top surface is 5.52m., and the maximum value of $|\tilde{w}|$ is .0062. In light of the constant θ calculation, it would appear that the variables $\tilde{u}, \tilde{w}$, and π are in quasi-steady equilibrium with respect to the θ field. (This problem of the slowly varying θ was discussed in Section II).

If one then assumes that the quasisteady model is producing a valid solution to the time-dependent problem, one then needs to ask whether or not the solution is physically meaningful. As discussed earlier, this question has not yet been

answered. If the answer is yes, one could develop reasonable confidence in the boundary conditions. If the answer is no, then one can reexamine various features of the model, such as the velocity input function, quasisteady forms of the characteristic equations, and boundary conditions. In any case, physical significance of the solution needs to be considered.

This problem was also solved with boundary conditions (4.2) and (4.3) at the top; eqs.(3.1) and (8) were used at the right boundary. With eq.(4.2) the wave propagates across the region in a reasonable fashion, but a significant overshoot in velocity (approximately 10%) occurs at the right corner point. It is not yet clear whether the problem is due to the boundary conditions or to the corner point equations.

With eq.(4.3) the wave propagates across the field at a much slower velocity. This can be seen from Figure 19, which displays the velocity profiles at $\zeta = 0$ for the two cases at a fixed time. The solution with eq.(4.3) displays another interesting characteristic: Rather than achieving a steady-state, the flow continues to push upward into the undisturbed flow. Figure 20 shows the horizontal velocity at $\zeta = 1$. Near $\eta = 0$ the flow appears to achieve a linear profile rather than a constant profile. This, then, produces a non-zero vertical velocity near $\eta = 0$, and this in turn allows the flow to push upward into the region. This upward motion, in terms of the position of the top surface, is shown in Figure 21. It is conceivable that an appropriate incoming lateral flow could move vertically into the less dense fluid, rather than propagate horizontally. Boundary condition (4.3) could be suitable for this type of flow.

Section VII: Conclusions

For the most part this study is based on the following two assumptions:

1) A boundary condition, by its very nature, must reflect a physical assumption in regard to the external flow configuration. Consequently, a proposed physical interpretation should be associated with any proposed boundary condition.

2) Eq.(3) is to be solved in a region of height h and length L, with $h \ll L$. It is assumed that boundary conditions and initial conditions to be imposed on Eq.(3) are such that the flow variables will experience significant variations only over time scales which are large compared to h/L.

Remark: The second of the above is the basic scale assumption, and was formulated in ref.[1] as assumption (2).

A primary purpose of this paper was to investigate the validity of the following hypotheses:

i) There exists a significant lack of physical understanding in regard to several relatively simple flows in an atmospheric environment. This situation seriously hampers the process of specifying and evaluating boundary conditions to be used in mathematical models for large-scale atmospheric flow.

ii) Assume that Eq.(3), together with a given set of boundary and initial conditions, defines a well-posed mathematical problem. It is then possible, by consistently applying the above assumption (2) to both the partial differential equations and the boundary conditions, to obtain well-posed mathematical models whose time-dependent scale is suitable for large-scale atmospheric flow.

In support of the first hypothesis, the following specific points are noted:

a) Because of the slow reaction time for θ, it appears that actual steady-state solutions cannot be reached in the time scale of these problems. This behavior of θ needs to be factored into the physical interpretation of the problem.

b) In the problem of a wave entering at a lateral boundary, several factors may significantly affect the profile of the propagating waves. These factors include the height of the region of entry and the choice of the upper boundary condition. Mathematically, all solutions seemed reasonable. Consequently, further evaluation requires more physical input regarding definition of the problem.

c) In Section IV an example was described in which the solution, although reasonable mathematically, did not agree with the solution for the extended region. Again, physical input (which was not postulated for this particular set of boundary conditions) is required.

In support of the second hypothesis, the following specific points are noted:

a) The quasisteady model operates on a time-scale suitable for large-scale atmospheric flow.

b) All solutions were shown to be stable and continuously dependent on the data. (In ref.[1] it was indicated that convergence in terms of a decreasing mesh size is a test of stability).

c) All solutions shown appear to have a sensible physical interpretation. However, in one problem (see Section VI) an overshoot occurred at a corner point; this might indicate that, for this choice of boundary conditions, the quasisteady limit was not taken correctly.

d) The proposed lateral boundary conditions behaved well and it was shown that they could be interpreted physically. In particular, the comparison with solutions for an extended region was very satisfactory.

Acknowledgement

This work has been supported by the office of Naval Research, Fluid Dynamics Program.

References

1. P. Gordon, "Quasisteady Primitive Equations with Associated Upper Boundary Conditions", J. Math. Physics, v.20, April, 1979.

2. S. M. Scala and P. Gordon, "Solutions of the Time-Dependent Navier-Stokes Equations for the Flow Around a Circular Cylinder", AIAA Journal, Jan., 1967.

3. R. Courant and D. Hilbert, Methods of Mathematical Physics (v.2, Partial Differential Equations, Interscience Publishers, New York, 1962.

4. J. H. Chen, "Numerical Boundary Conditions and Computational Modes", J. of Computational Physics, v. 13, no. 4, 1973, pp. 522-535.

5. O. Belotserkovskii, "New Computational Methods in Continuum Mechanics", University of Maryland, College Park, Department of Aerospace Engineering, Technical Report No. AE-79-1, March, 1979.

6. A. Sundström, "Boundary Conditions for Limited-Area Integration of the Viscous Forecast Equations", Beiträge zur Physik der Atmosphäre, 50. Band, 1977, Seite 218-224.

7. H. C. Davies, "On the Initial-Boundary Value Problem of Some Geophysical Fluid Flows", Journal of Computational Physics, v. 13, 1973, pp. 398-422.

8. J. S. Bramley and D. M. Sloan, "A Comparison of Boundary Methods for the Numerical Solution of Hyperbolic Systems of Equations", J. of Engineering Mathematics, v. 11, no. 3, 1977.

9. J. Oliger and A. Sundström, "Theoretical and Practical Aspects of Some Initial-Boundary Value Problems in Fluid Dynamics", Stanford University Computer Science Dept., Rep. STAN-CS-76-578, Nov., 1976.

10. Jacques Hadamard, Lectures on Cauchy's Problem in Linear Partial Differential Equations, Dover Publications, 1952, New York.

11. I. Orlanski, "A simple Boundary Condition for Unbounded Hyperbolic Flows", J. Comput. Physics, v. 21, pp. 251-269.

12. D. J. Perkey and C. W. Kreitzberg, "A Time-Dependent Lateral Boundary Scheme for Limited-Area Primitive Equation Models", Mon. Wea. Rev., v. 104, 1975.

13. J. B. Klemp and D. K. Lilley, "Numerical Simulation of Hydrostatic Mountain Waves", J. of the Atmospheric Sciences, v. 35, 1978, pp. 78-107.

14. P. Gordon and S. M. Scala, "Nonlinear Theory of Pulsatile Blood Flow Through Viscoelastic Blood Vessels", Proceedings of the AGARD Specialists' Meeting on Fluid Dynamics of Blood Circulation and Respiratory Flow, 4-6 May, 1970, Naples, Italy, Technical Editing and Reproduction Ltd., London, 1970.

15. S. M. Scala, et al, "Studies of Blood Flow In and Adjacent to Blood Pumps" Annual Report, June, 1970, Artificial Heart Program, Grant No. PH-43-67-1121.

Figure 1: Initial Flow Field

$\theta(0,x,z)$

$\frac{z}{10\ km.}$													
1.	1.2670	1.2670	1.2670	1.2670	1.2670	1.2670	1.2670	1.2670	1.2670	1.2670	1.2670	1.2670	1.2670
.75	1.1600	1.1602	1.1608	1.1617	1.1628	1.1641	1.1654	1.1668	1.1681	1.1692	1.1701	1.1707	1.1709
.50	1.0935	1.0941	1.0956	1.0976	1.1006	1.1038	1.1072	1.1106	1.1138	1.1166	1.1189	1.1203	1.1209
.25	1.0595	1.0601	1.0618	1.0642	1.0673	1.0708	1.0744	1.0781	1.0816	1.0847	1.0871	1.0888	1.0893
0.	1.0500	1.0500	1.0500	1.0500	1.0500	1.0500	1.0500	1.0500	1.0500	1.0500	1.0500	1.0500	1.0500

$\pi(0,x,z)$

1.	.68721	.68721	.68721	.68721	.68721	.68721	.68721	.68721	.68721	.68721	.68721	.68721	.68721
.75	.76193	.76092	.76090	.76087	.76083	.76079	.76075	.76070	.76066	.76062	.76060	.76058	.76057
.50	.84123	.84020	.84010	.83996	.83978	.83958	.83937	.83916	.83896	.83878	.83864	.83855	.83852
.25	.92318	.92311	.92289	.92257	.92217	.92171	.92123	.92076	.92031	.91992	.91960	.91940	.91932
0.	1.00783	1.00773	1.00745	1.00703	1.00651	1.00592	1.00529	1.00467	1.00409	1.00359	1.00318	1.00291	1.00282

$P(0,x,z)$

1.	269.039	269.039	269.039	269.039	269.039	269.039	269.039	269.039	269.039	269.039	269.039	269.039	269.039
.75	384.325	384.313	384.278	384.226	384.160	384.086	384.008	383.930	383.856	383.792	383.740	383.706	383.694
.50	543.744	543.666	543.452	543.129	542.726	542.271	541.791	541.314	540.866	540.473	540.160	539.954	539.879
.25	755.976	755.753	755.139	754.216	753.064	751.765	750.398	749.040	747.767	746.653	745.768	745.185	744.974
0.	1027.670	1027.310	1026.316	1024.822	1022.959	1020.858	1018.650	1016.457	1014.403	1012.604	1011.177	1010.236	1009.897

$T(0,x,z)$

1.	237.831	237.831	237.831	237.831	237.831	237.831	237.831	237.831	237.831	237.831	237.831	237.831	237.831
.75	241.105	241.147	241.264	241.440	241.661	241.912	242.178	242.444	242.694	242.916	243.092	243.209	243.251
.50	250.977	251.090	251.403	251.876	252.468	253.141	253.853	254.565	255.237	255.829	256.302	256.614	256.727
.25	267.183	267.319	267.655	268.178	268.835	269.579	270.367	271.156	271.900	272.555	273.078	273.424	273.549
0.	289.053	289.024	288.944	288.824	288.674	288.504	288.326	288.146	287.982	287.836	287.720	287.643	287.616

0.	.08333	.16667	.25	.33333	.41667	.50	.58333	.66667	.75	.83333	.91667	1.

$\left(\frac{x}{480.\ km.}\right)$

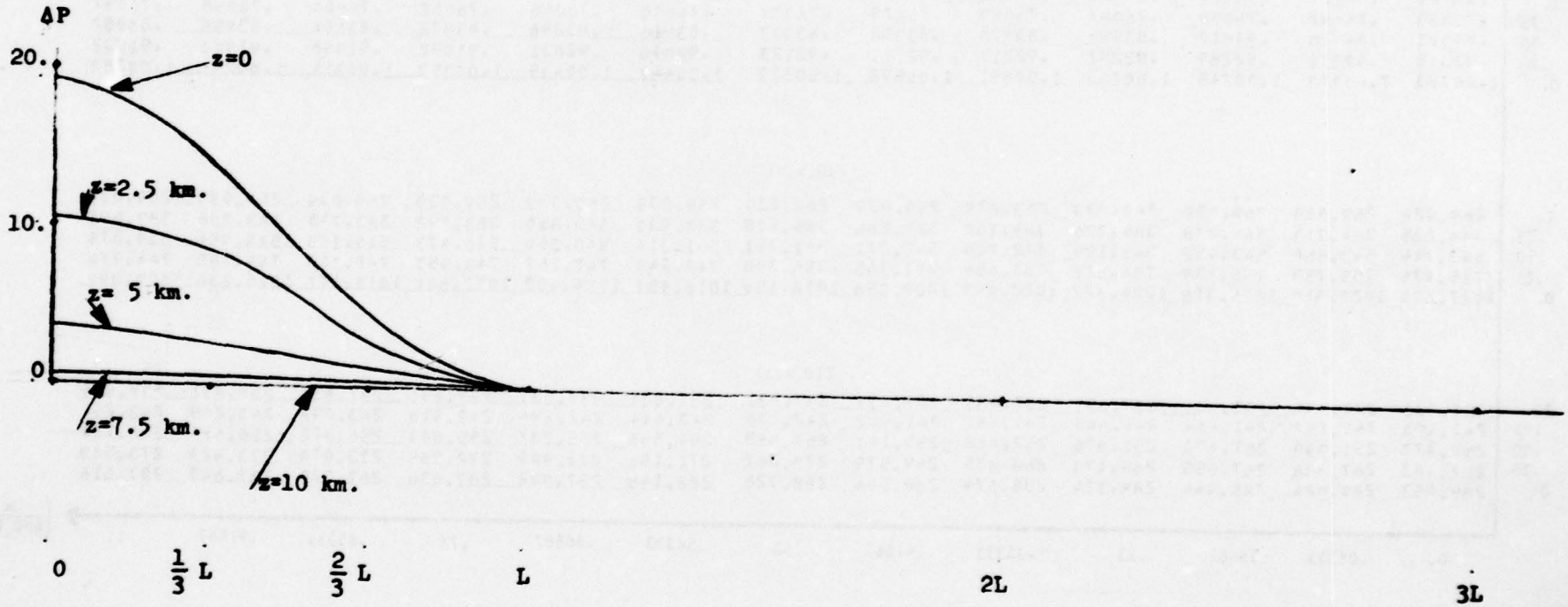

FIGURE 2: OVERPRESSURE AT INITIAL TIME: $\Delta P = P(0,x,z) - P(0,L,z)$

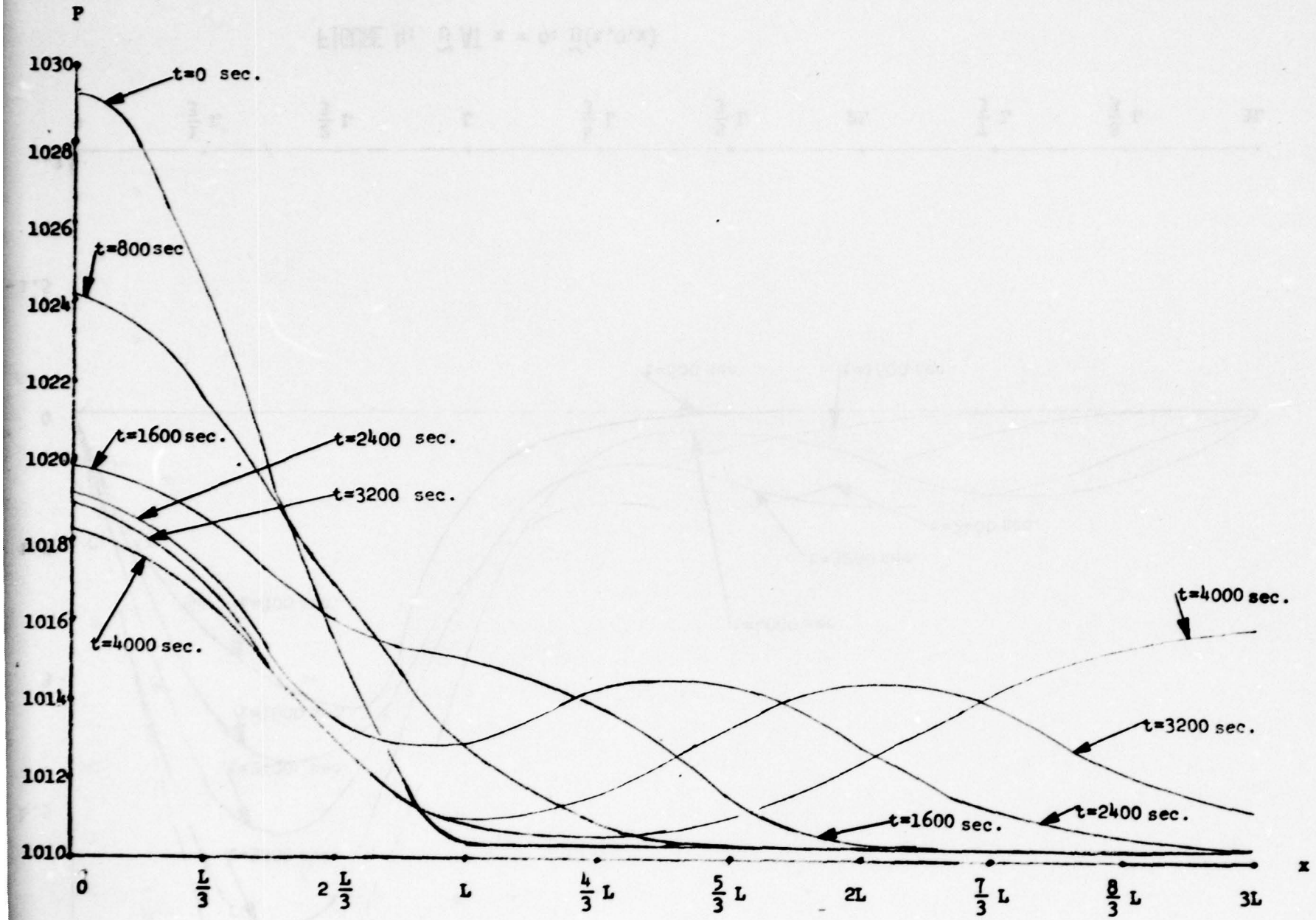

FIGURE 3: P(t,x,0)

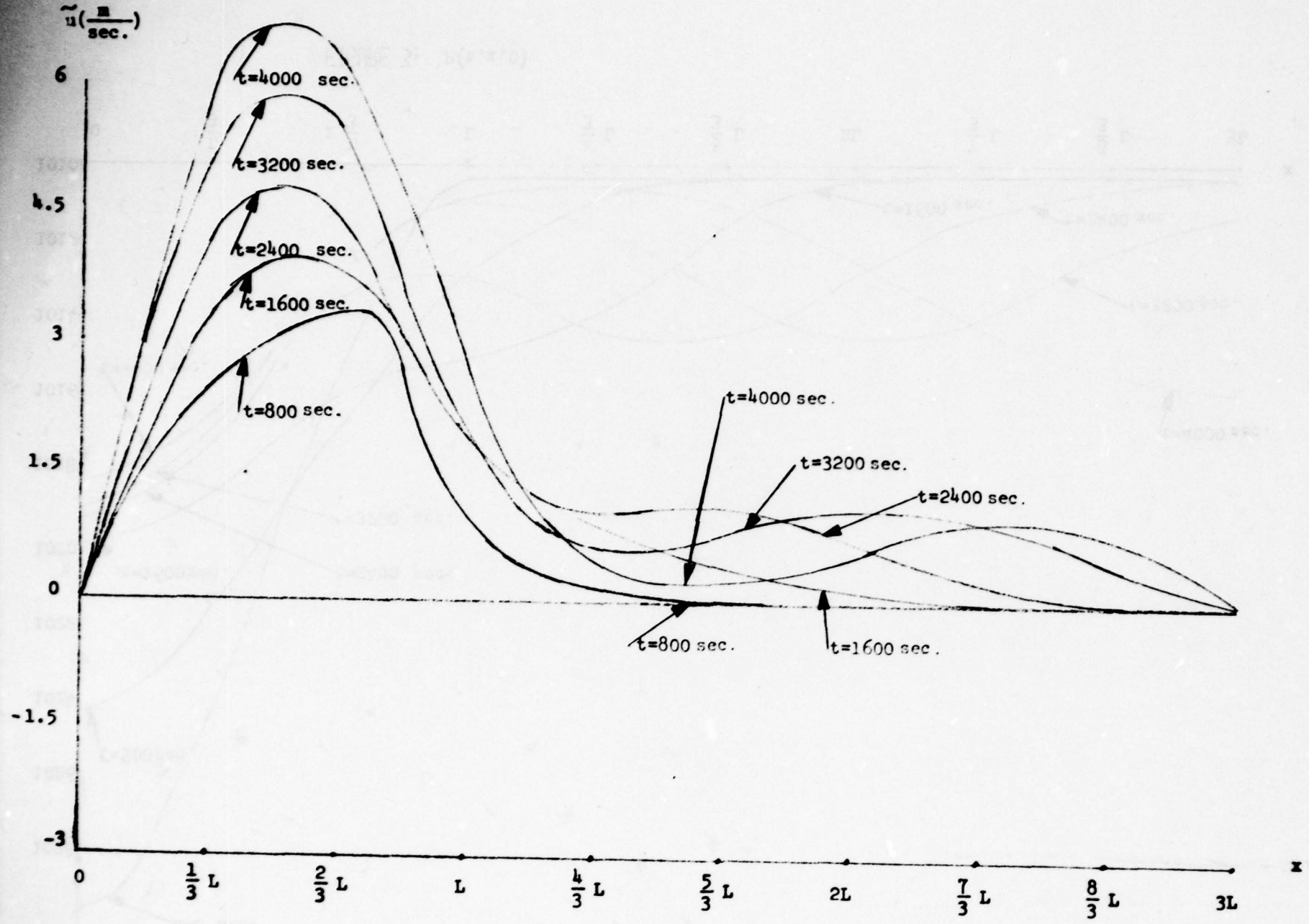

FIGURE 4: $\tilde{u}$ AT z = 0: $\tilde{u}(t,0,x)$

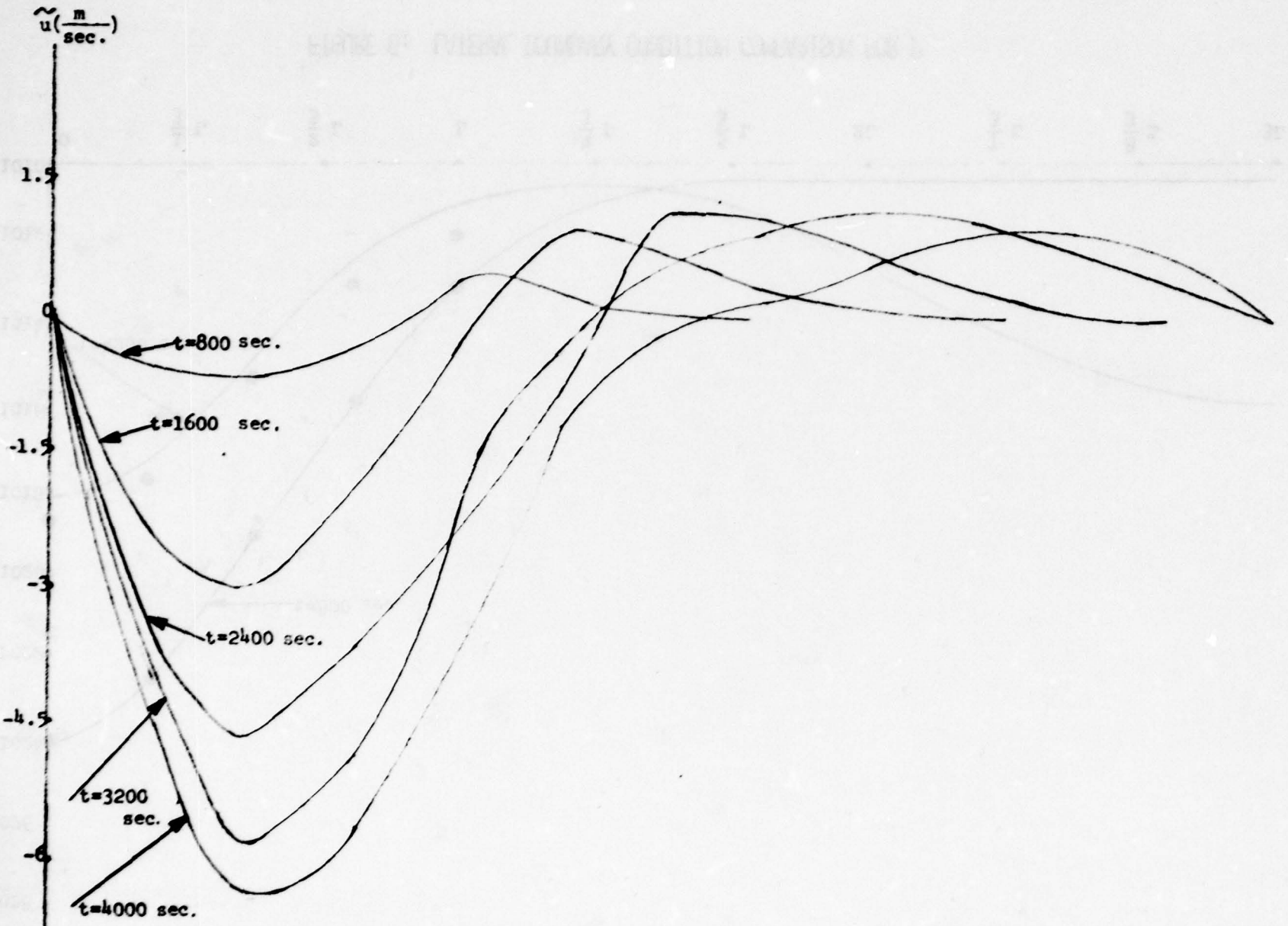

FIGURE 5: $\tilde{u}$ AT TOP SURFACE

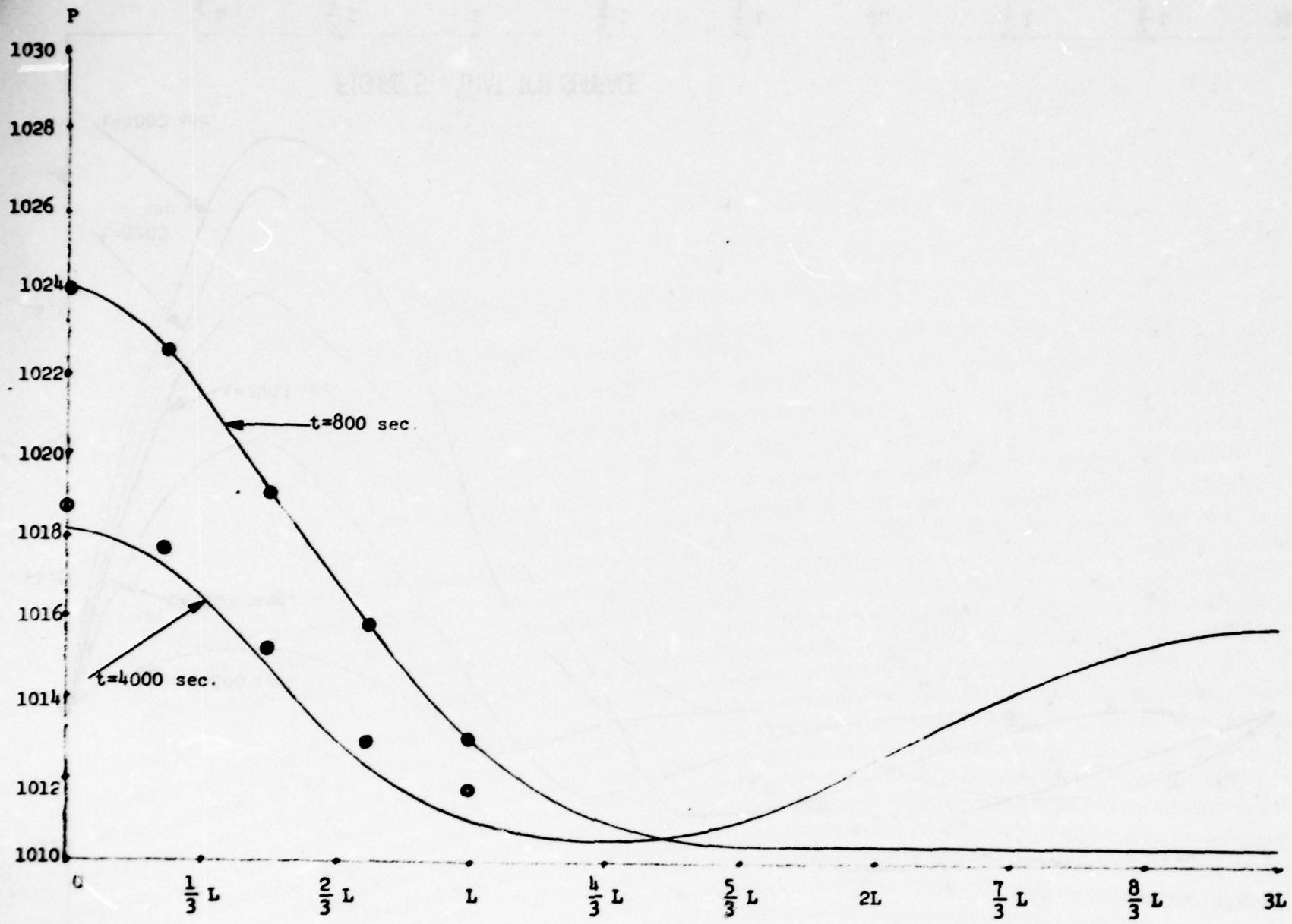

FIGURE 6: LATERAL BOUNDARY CONDITION COMPARISON FOR P

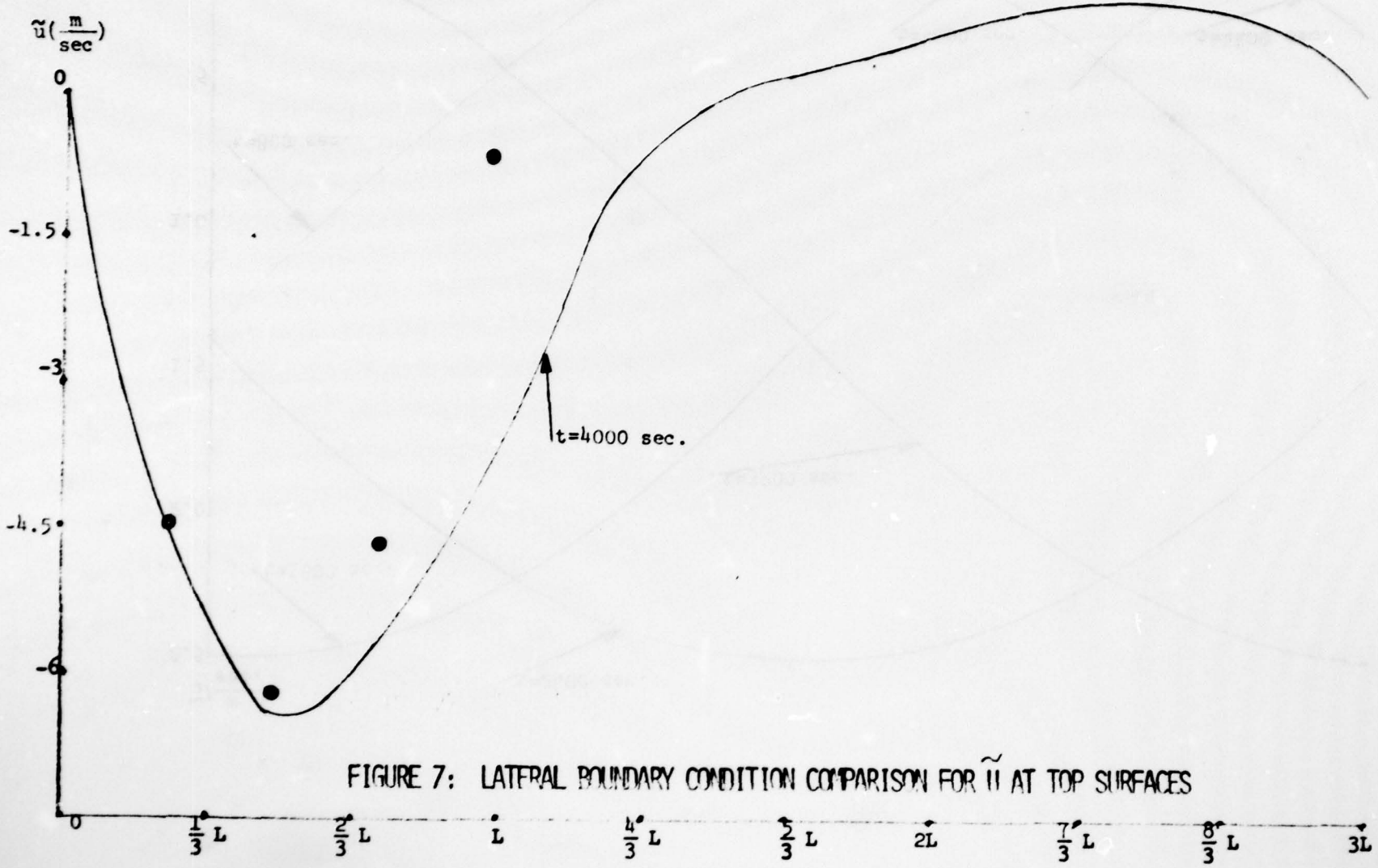

FIGURE 7: LATERAL BOUNDARY CONDITION COMPARISON FOR $\tilde{u}$ AT TOP SURFACES

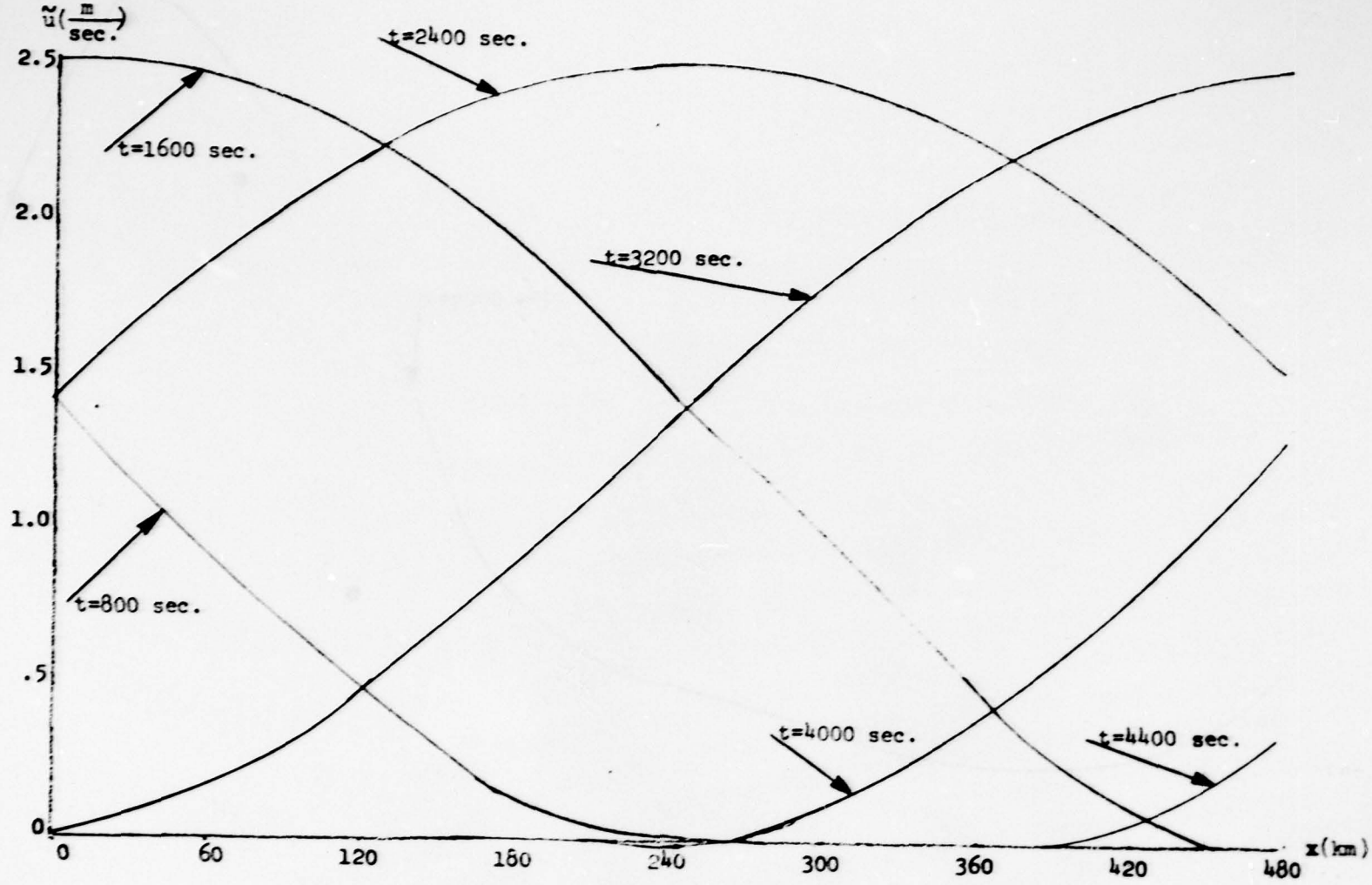

FIGURE 8: BELL-WAVE INPUT WITH UPPER BOUNDARY CONDITION EQ. (8)

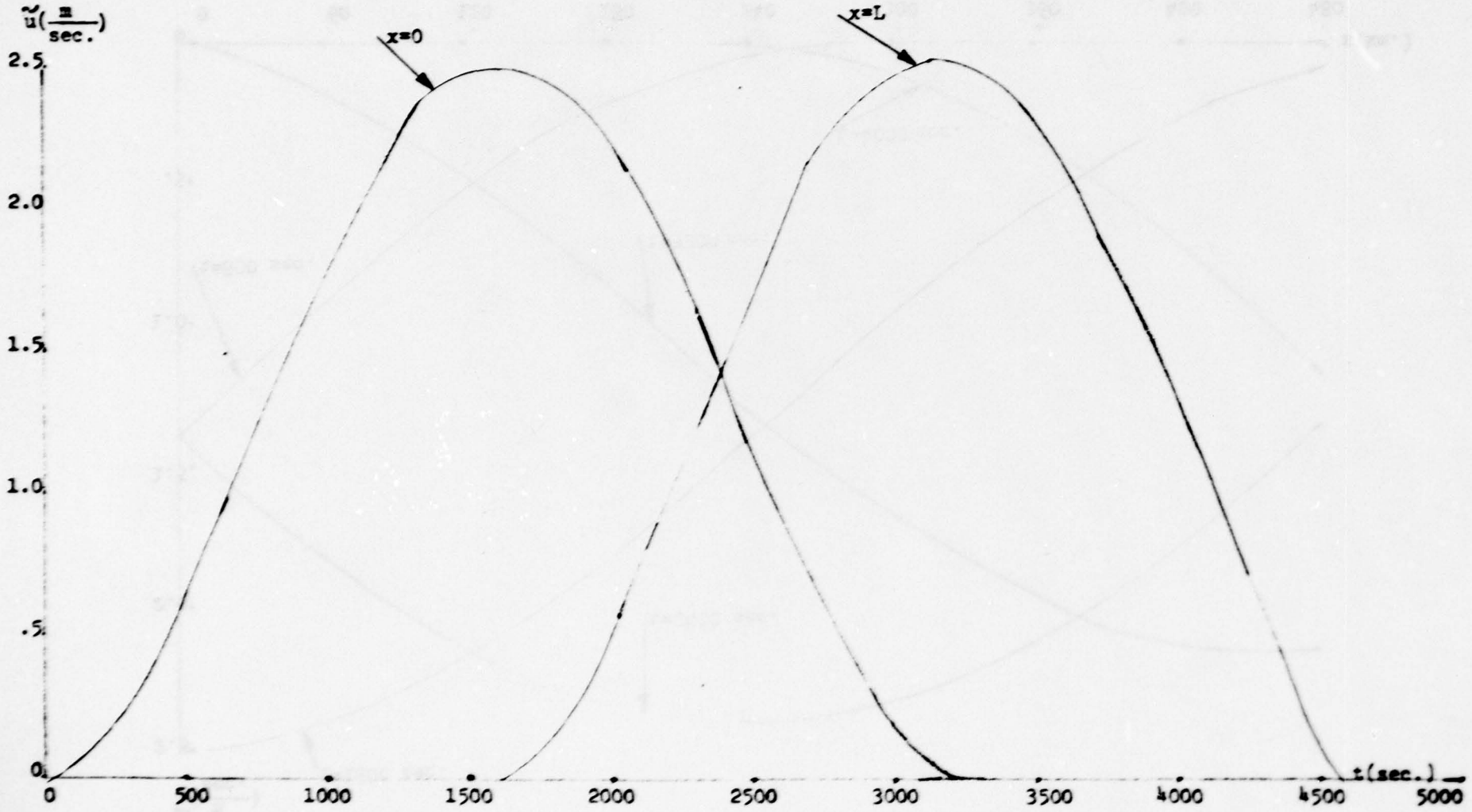

FIGURE 9: $\tilde{U}$ AT LATEPAL BOUNDARIES FOR UPPER BOUNDARY CONDITION EQ. (8)

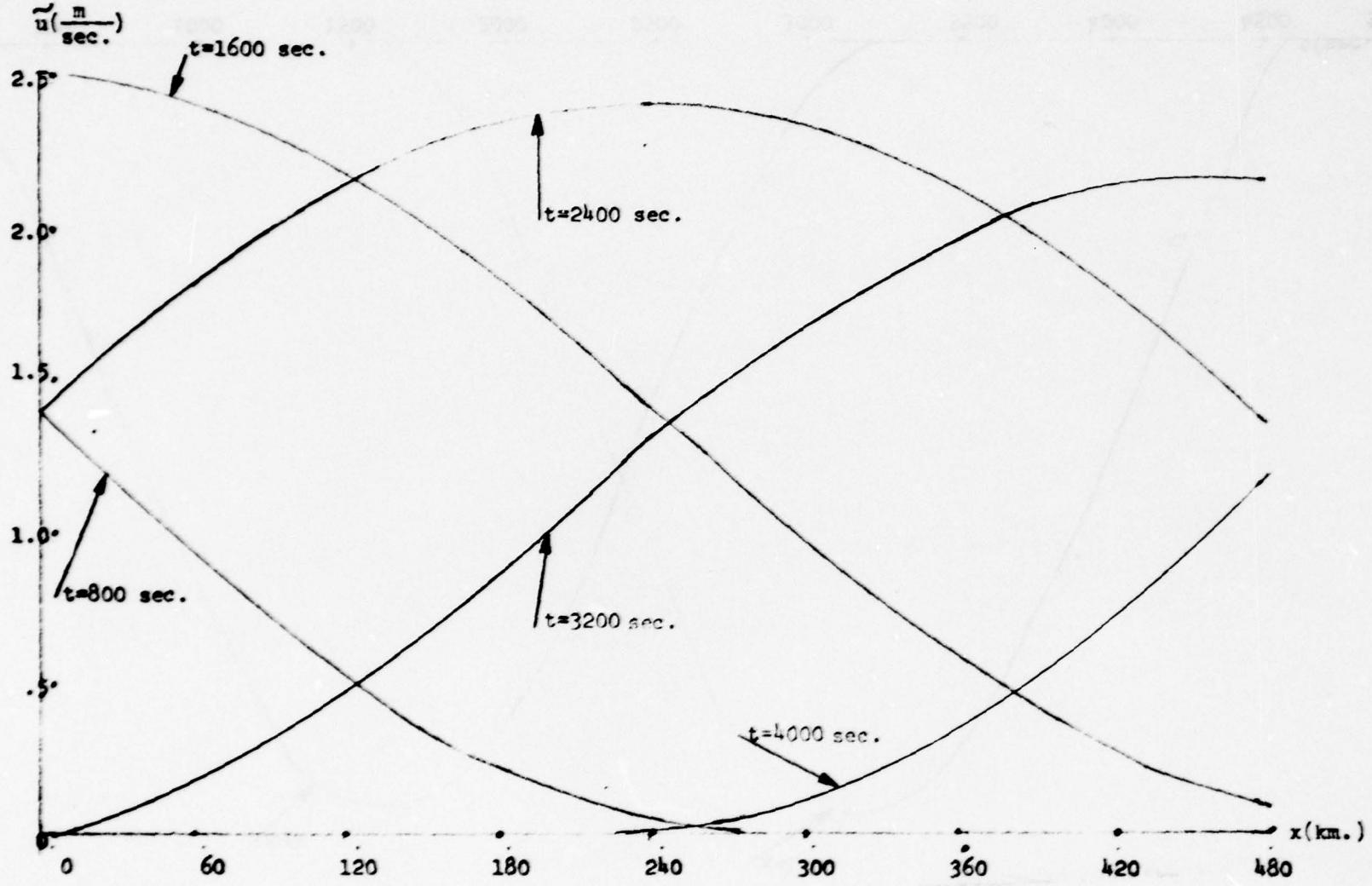

FIGURE 10: HORIZONTAL VELOCITY AT $z = 0$ FOR UPPER BOUNDARY CONDITION 4.2

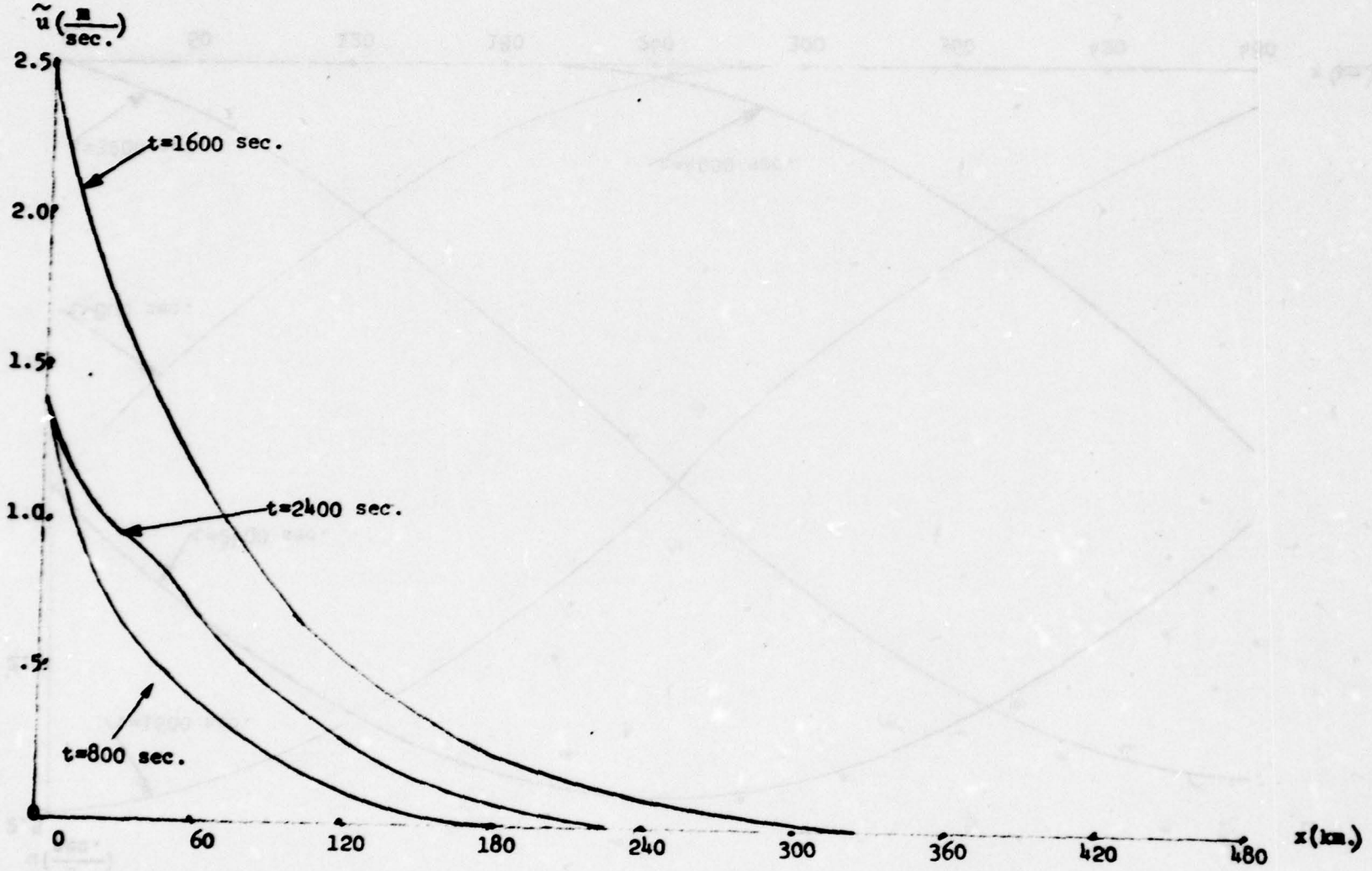

FIGURE 11: BELL-WAVE INPUT WITH UPPER BOUNDARY CONDITION 4.3

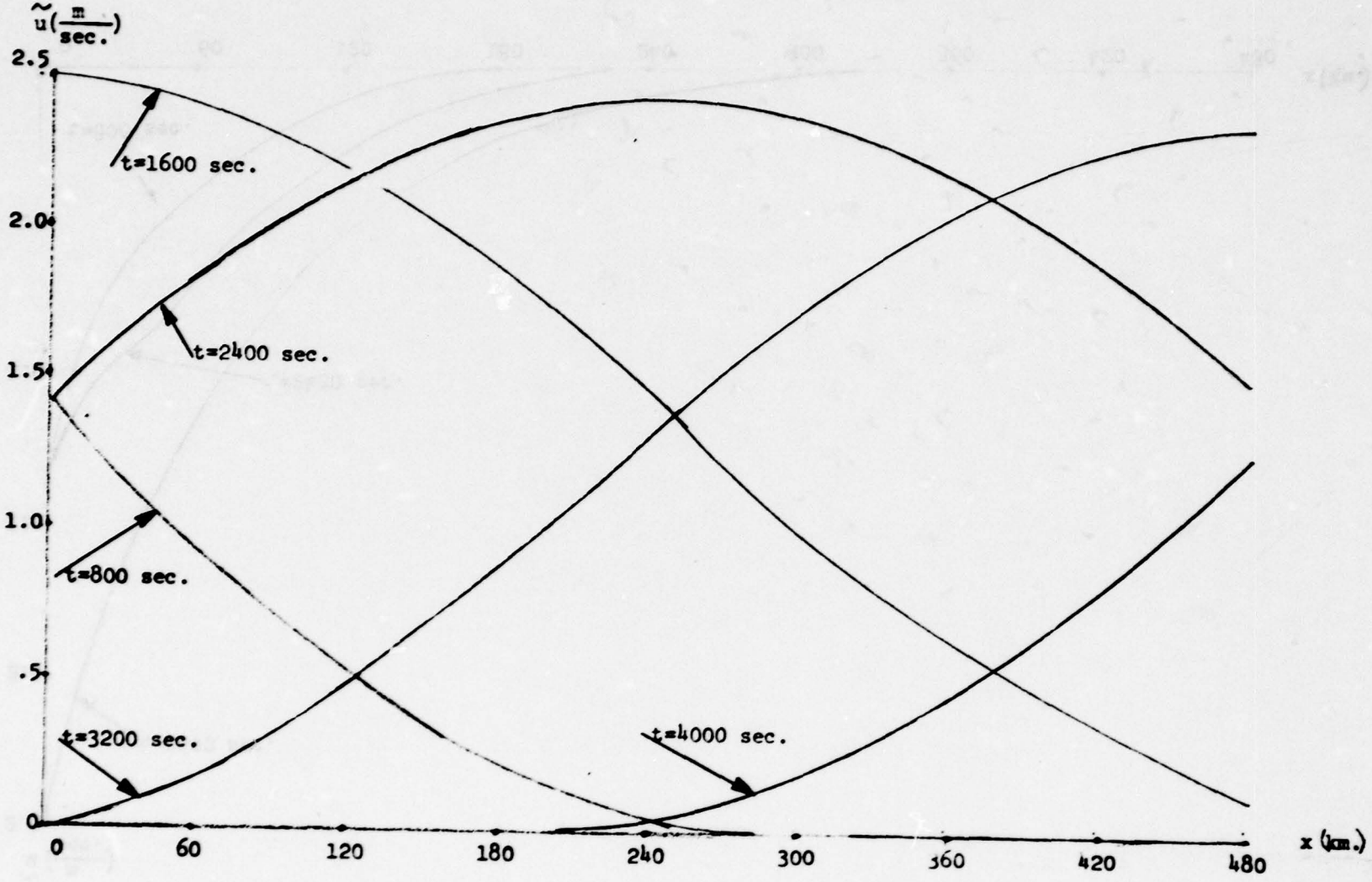

FIGURE 12: COMBINED UPPER BOUNDARY CONDITION

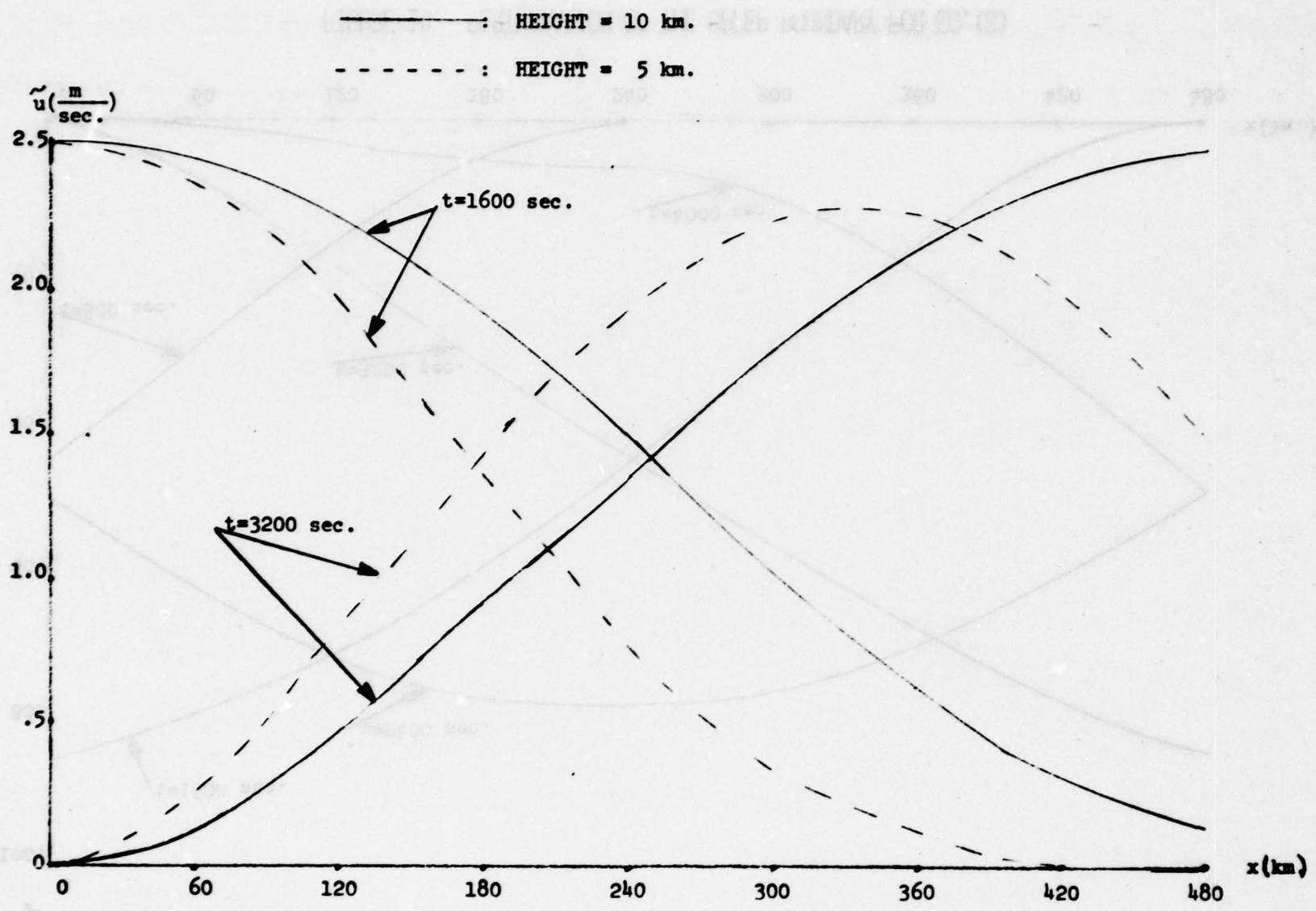

FIGURE 13: EFFECT OF HEIGHT WITH UPPER BOUNDARY CONDITION 4.2

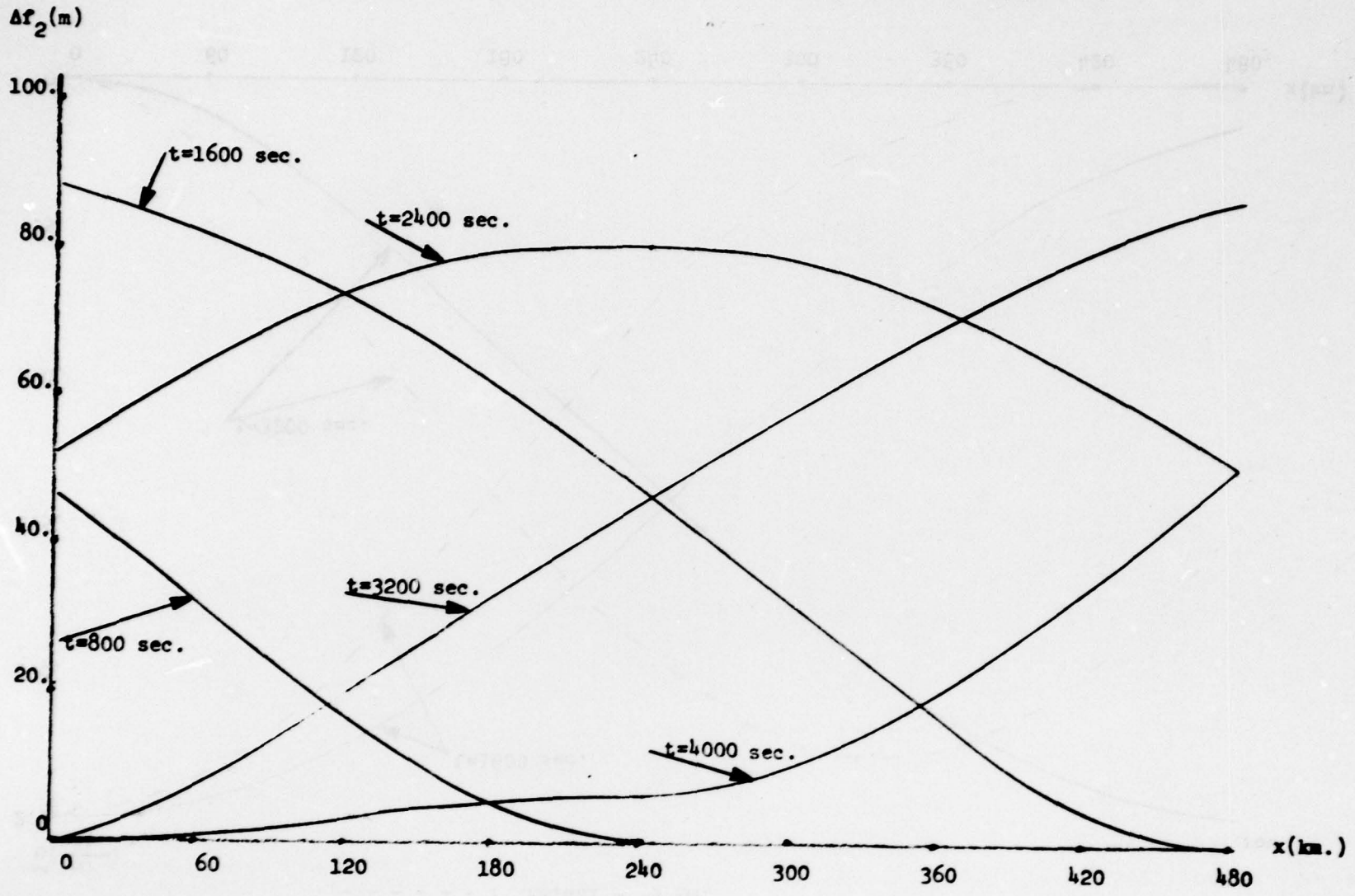

FIGURE 14: PERTURBATION OF THE UPPER BOUNDARY FOR EQ. (8)

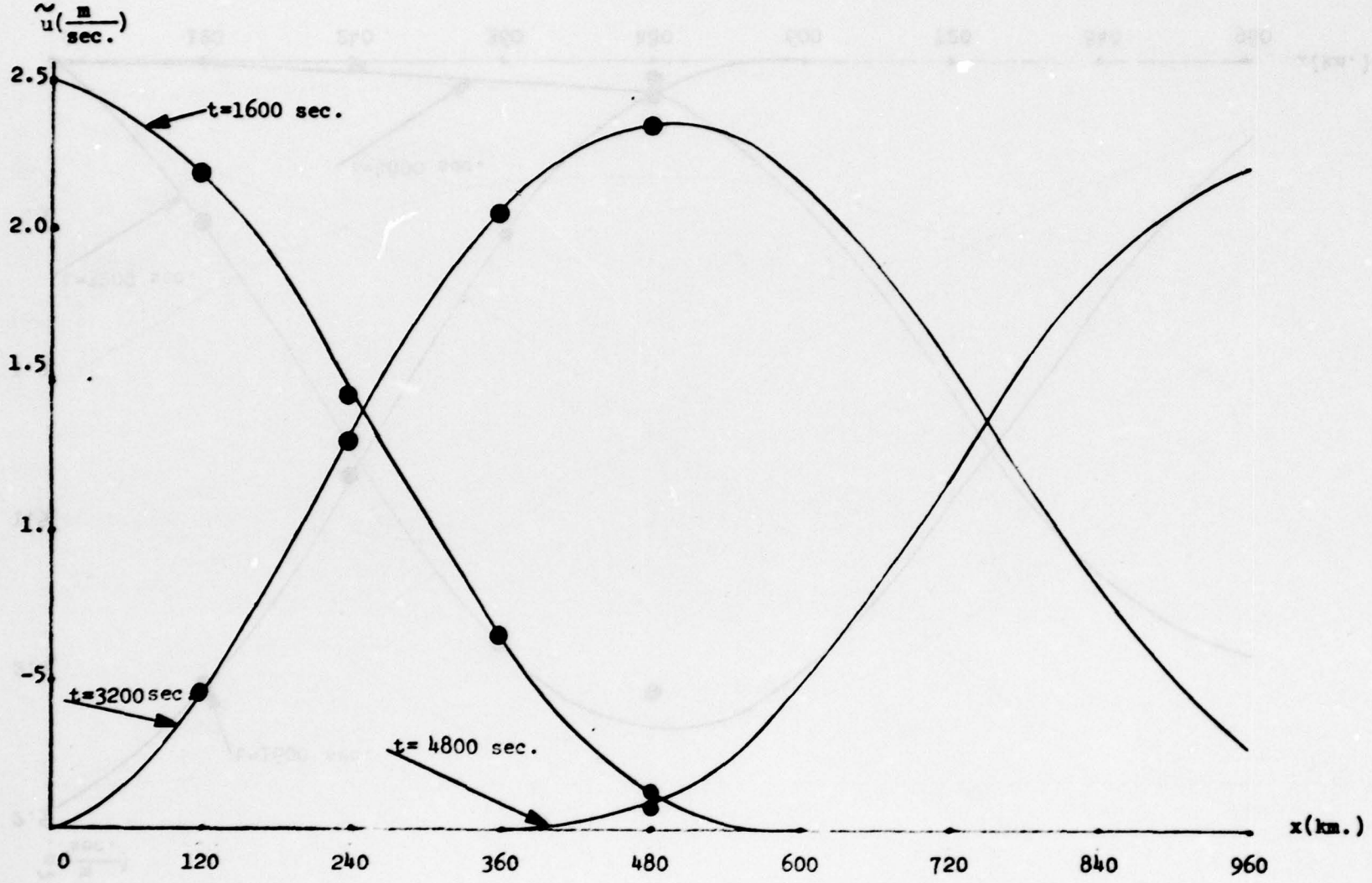

FIGURE 15: COMPARISON WITH DOUBLED LENGTH AT $\zeta = 1$

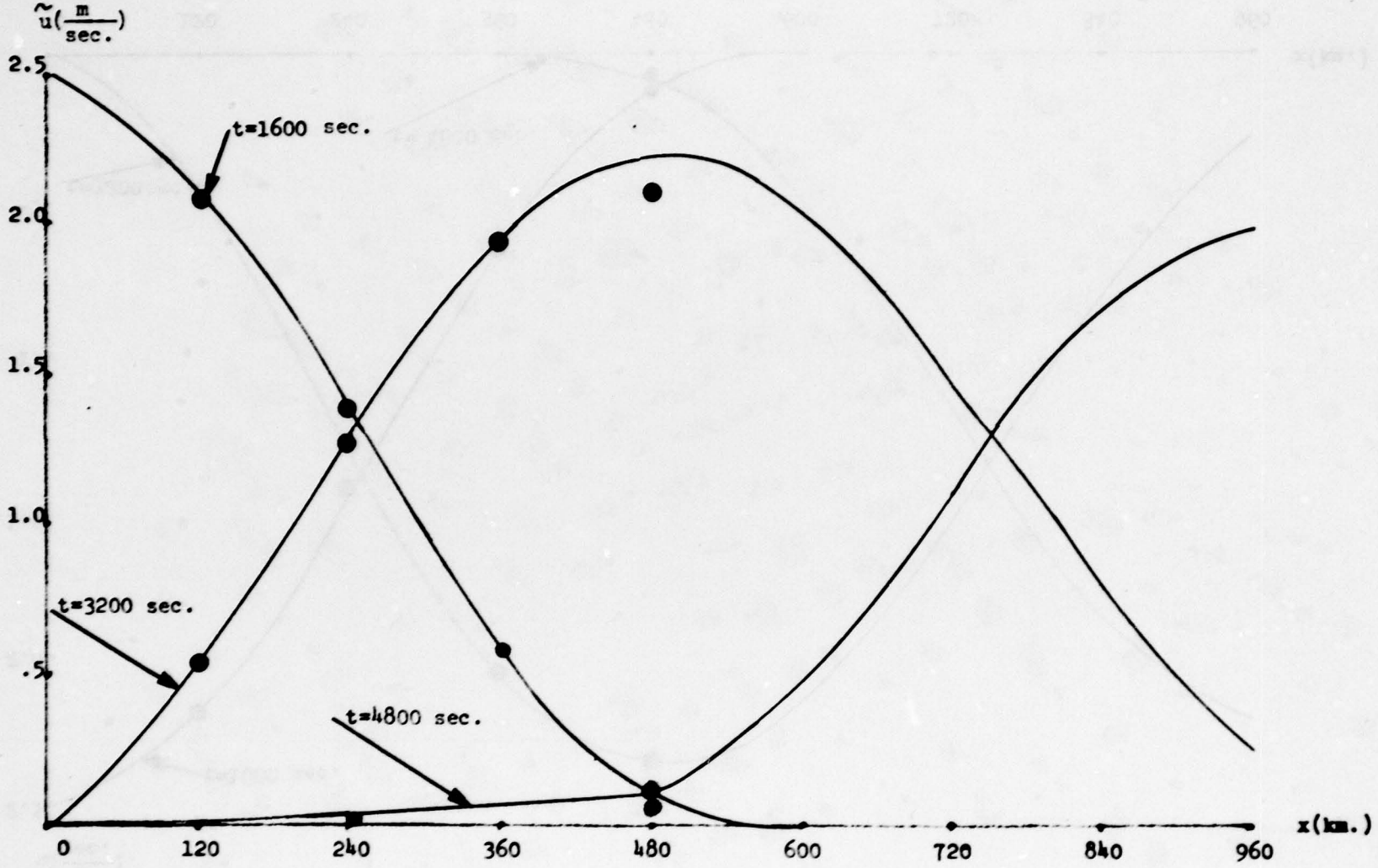

FIGURE 16: COMPARISON WITH DOUBLED LENGTH AT $\tau = 0$

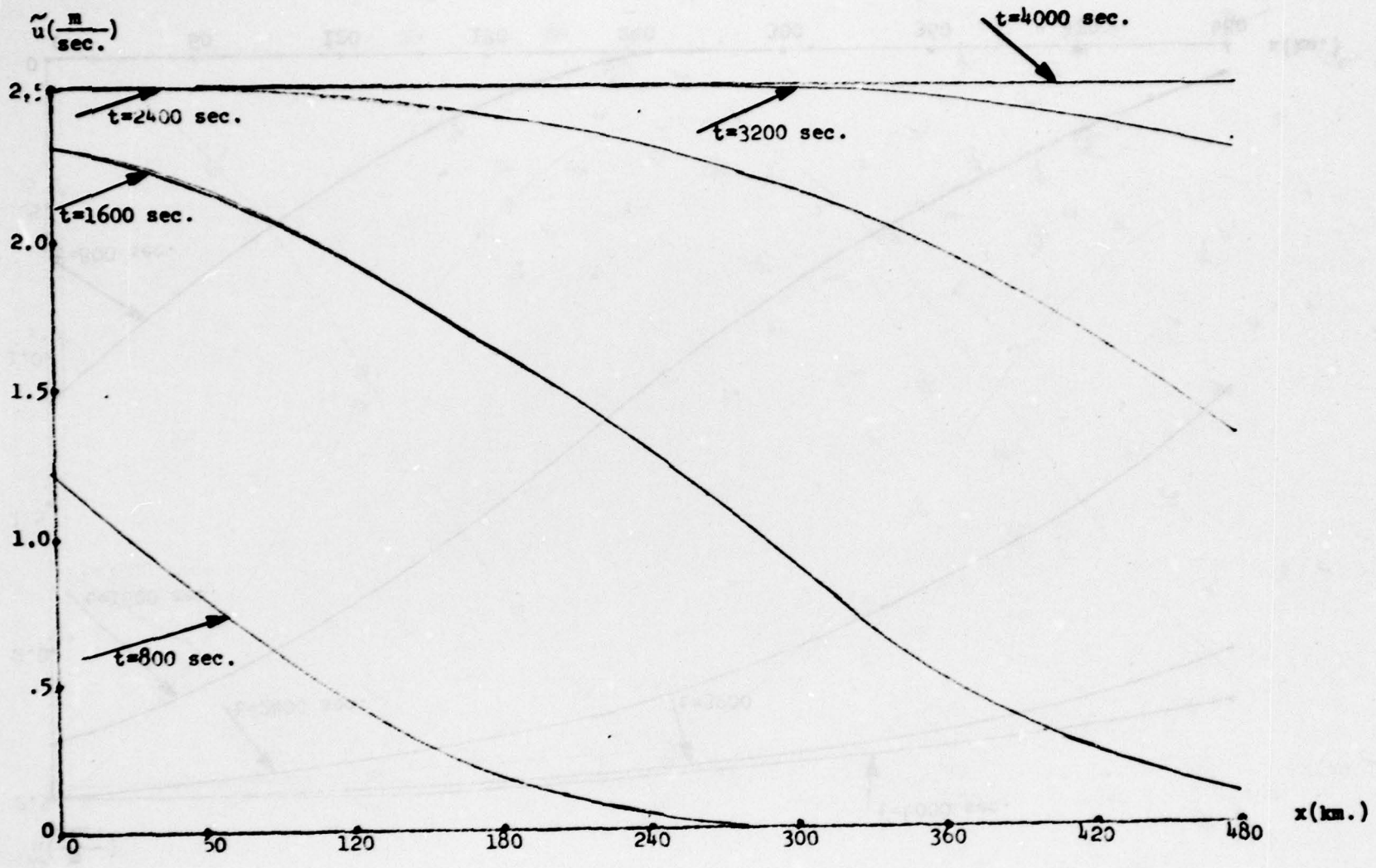

FIGURE 17: HORIZONTAL VELOCITY AT TOP SURFACE

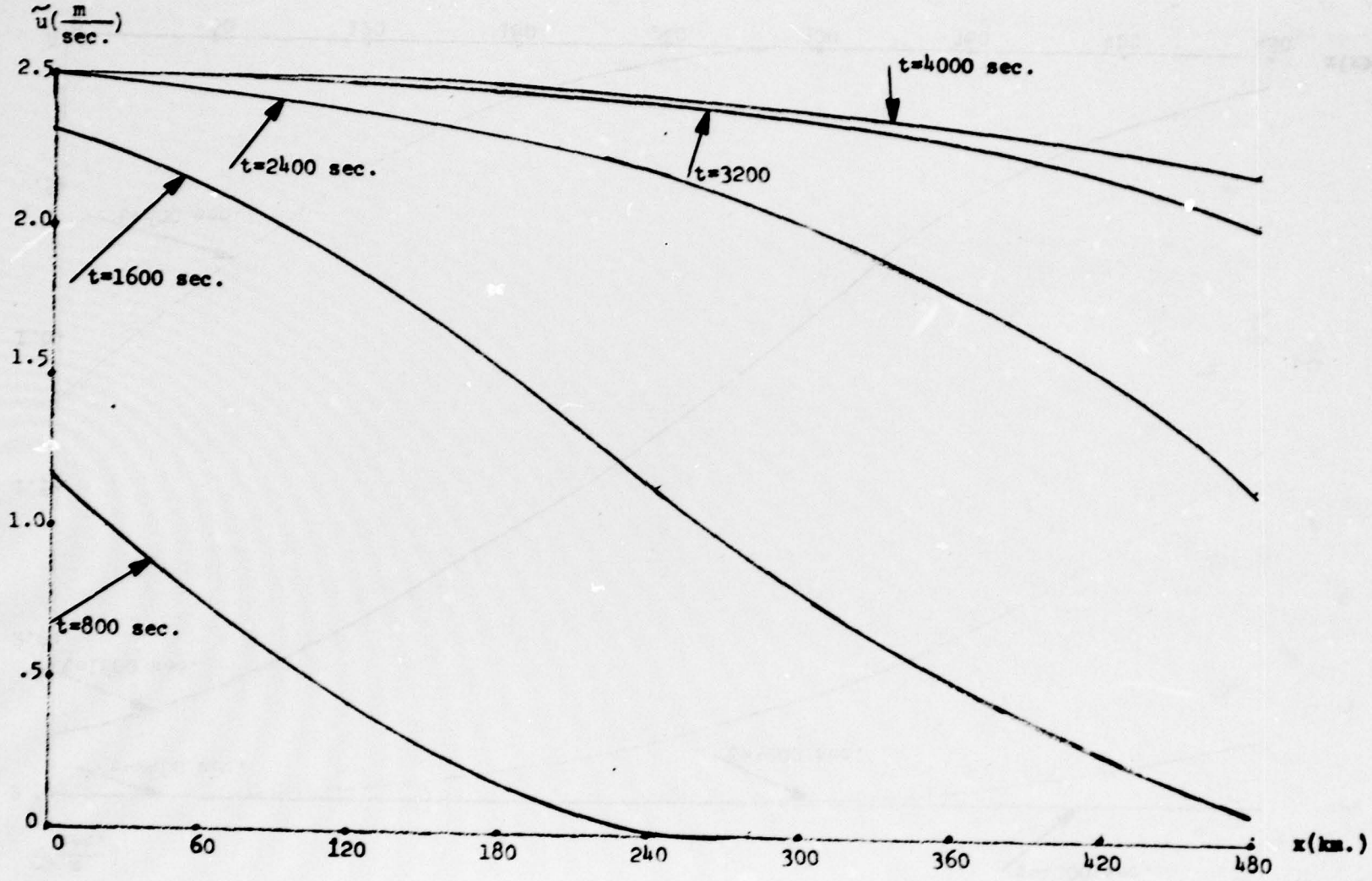

FIGURE 18: HORIZONTAL VELOCITY AT BOTTOM SURFACES

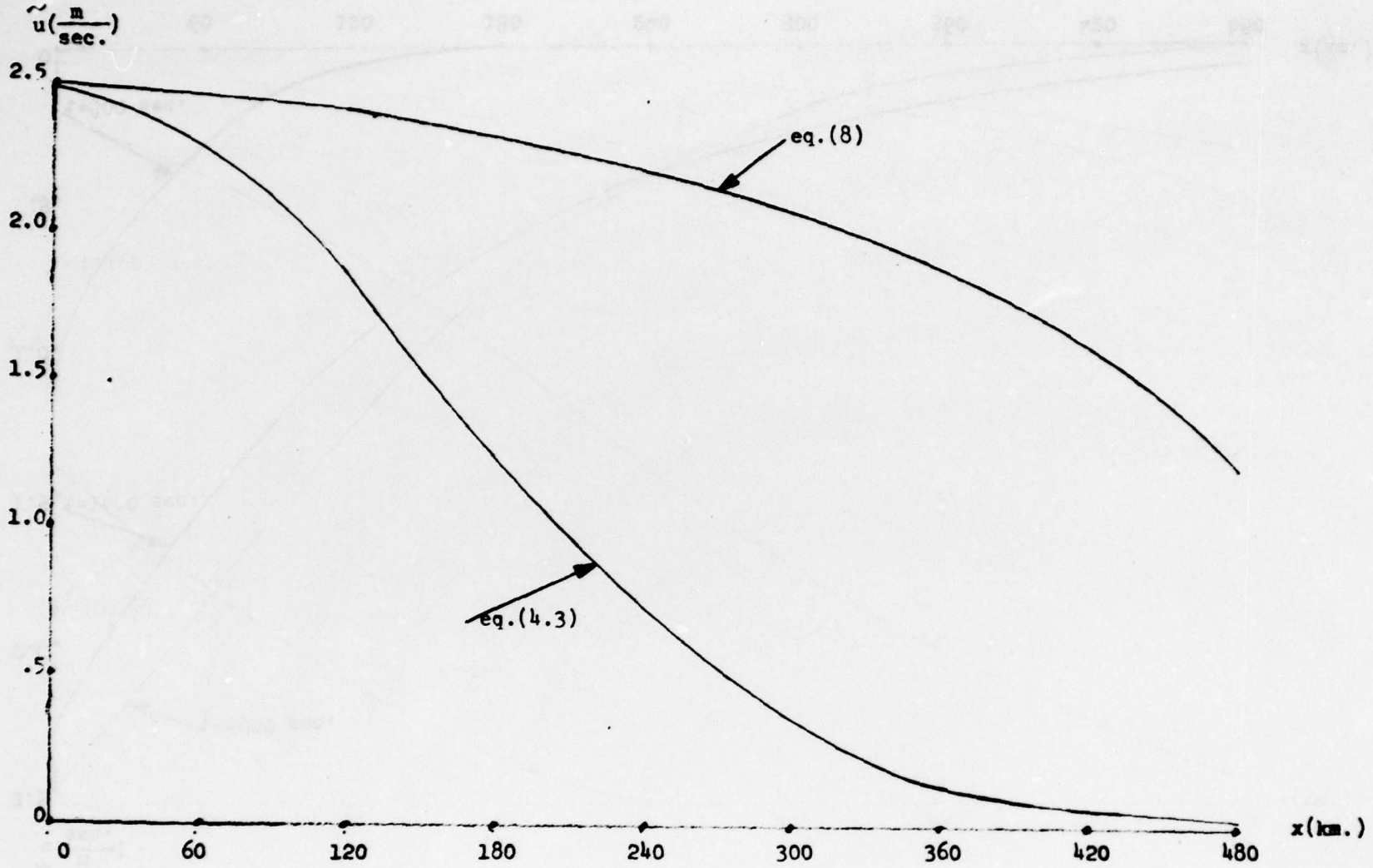

FIGURE 19: VELOCITY AT $\tau = 0$, $T = 240$ SEC.

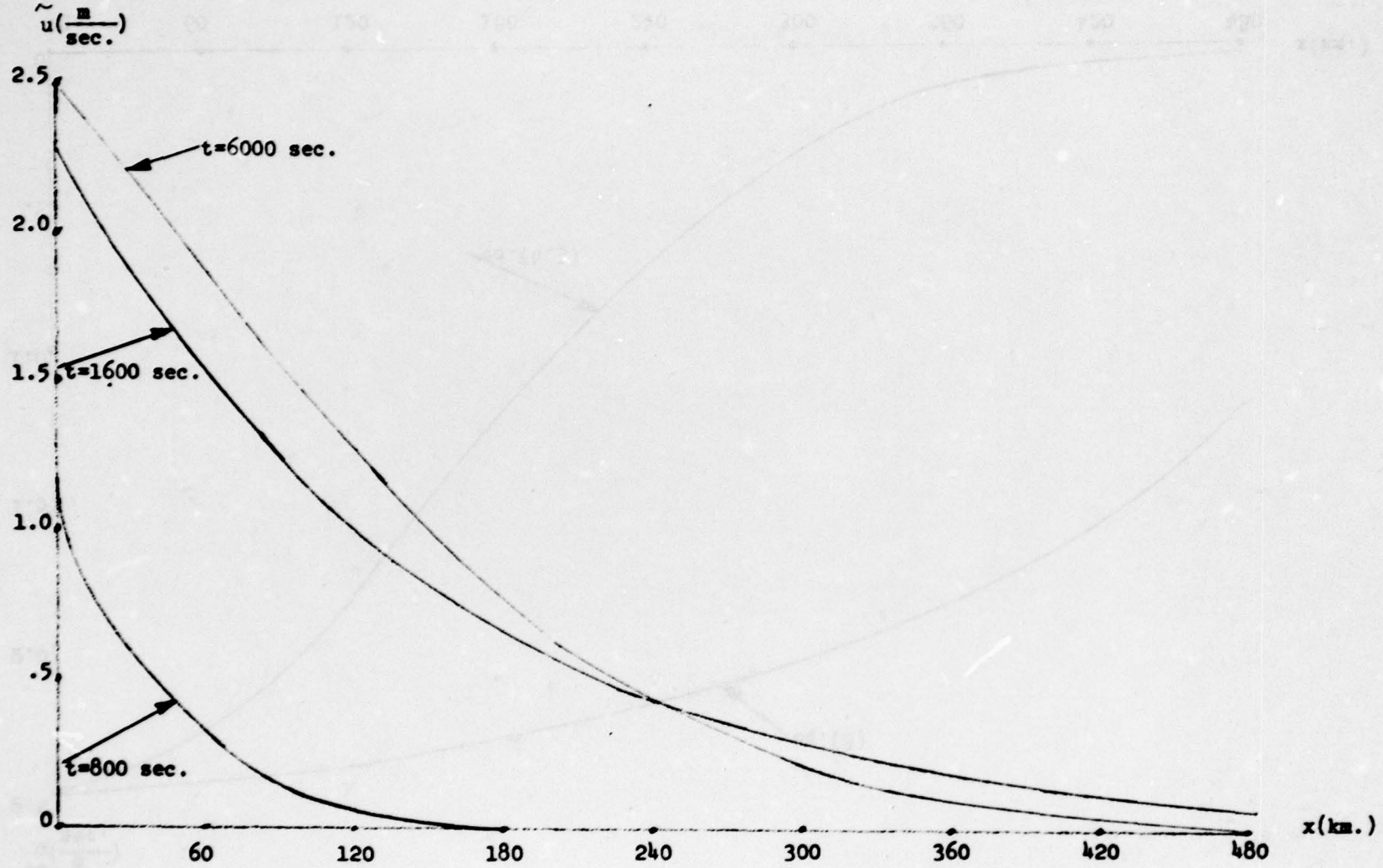

FIGURE 20: $\tilde{U}$ AT $\tau = 1$

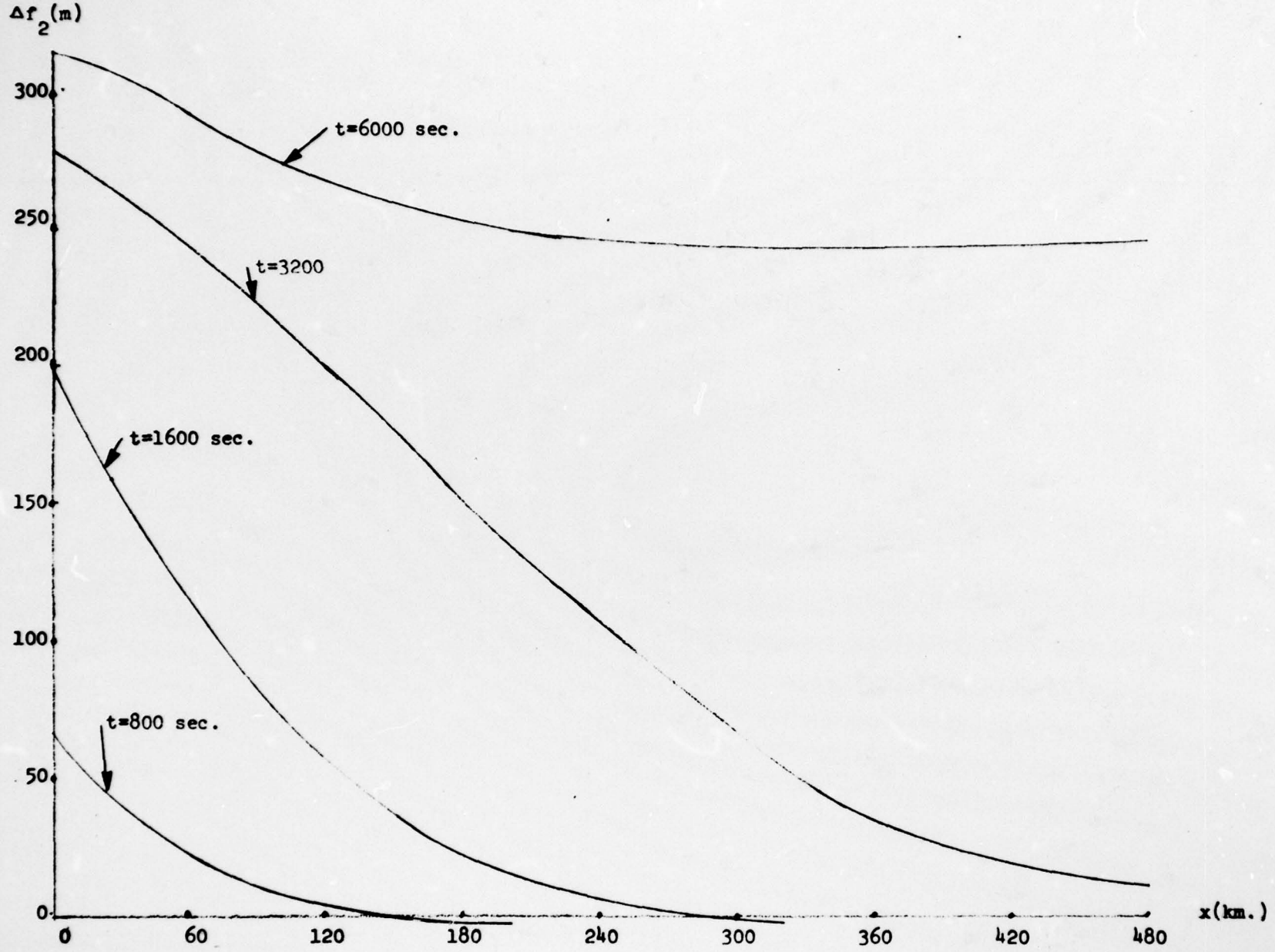

FIGURE 21: POSITION OF TOP SURFACE

DISTRIBUTION LIST FOR UNCLASSIFIED
TECHNICAL REPORTS AND REPRINTS ISSUED UNDER
CONTRACT N00014-78-C-0305 TASK NR 061-254

All addresses receive one copy unless otherwise specified

Technical Library
Building 313
Ballistic Research Laboratories
Aberdeen Proving Ground, MD 21005

Dr. F. D. Bennett
External Ballistic Laboratory
Ballistic Research Laboratories
Aberdeen Proving Ground, MD 21005

Mr. C. C. Hudson
Sandia Corporation
Sandia Base
Albuquerque, NM 81115

Professor P. J. Roache
Ecodynamics Research
Associates, Inc.
P. O. Box 8172
Albuquerque, NM 87108

Dr. J. D. Shreve, Jr.
Sandia Corporation
Sandia Base
Albuquerque, NM 81115

Defense Documentation Center
Cameron Station, Building 5
Alexandria, VA 22314 12 copies

Library
Naval Academy
Annapolis, MD 21402

Director, Tactical Technology Office
Defense Advanced Research Projects
Agency
1400 Wilson Boulevard
Arlington, VA 22209

Office of Naval Research
Attn: Code 211
800 N. Quincy Street
Arlington, VA 22217

Office of Naval Research
Attn: Code 438
800 N. Quincy Street
Arlington, VA 22217

Office of Naval Research
Attn: Code 1021P (ONRL)
800 N. Quincy Street
Arlington, VA 22217 6 copies

Dr. J. L. Potter
Deputy Director, Technology
von Karman Gas Dynamics Facility
Arnold Air Force Station, TN 37389

Professor J. C. Wu
Georgia Institute of Technology
School of Aerospace Engineering
Atlanta, GA 30332

Library
Aerojet-General Corporation
6352 North Irwindale Avenue
Azusa, CA 91702

NASA Scientific and Technical
Information Facility
P. O. Box 8757
Baltimore/Washington International
Airport, MD 21240

Dr. K. C. Wang
Martin Marietta Corporation
Martin Marietta Laboratories
1450 South Rolling Road
Baltimore, MD 21227

Dr. S. A. Berger
University of California
Department of Mechanical Engineering
Berkeley, CA 94720

Professor A. J. Chorin
University of California
Department of Mathematics
Berkeley, CA 94720

Professor M. Holt
University of California
Department of Mechanical Engineering
Berkeley, CA 94720

Dr. H. R. Chaplin
Code 1600
David W. Taylor Naval Ship Research
and Development Center
Bethesda, MD 20084

Dr. Hans Lugt
Code 184
David W. Taylor Naval Ship Research
and Development Center
Bethesda, MD 20084

Dr. Francois Frenkiel
Code 1802.2
David W. Taylor Naval Ship Research
and Development Center
Bethesda, MD 20084

Dr. G. R. Inger
Department of Aerospace Engineering
Virginia Polytechnic Institute and
State University
Blacksburg, VA 24061

Professor A. H. Nayfeh
Department of Engineering Science
Virginia Polytechnic Institute and
State University
Blacksburg, VA 24061

Mr. A. Rubel
Research Department
Grumman Aerospace Corporation
Bethpage, NY 11714

Commanding Officer
Office of Naval Research Branch Office
666 Summer Street, Bldg. 114, Section D
Boston, MA 02210

Dr. G. Hall
State University of New York at Buffalo
Faculty of Engineering and Applied
Sciences
Fluid and Thermal Sciences Laboratory
Buffalo, NY 14214

Dr. R. J. Vidal
CALSPAN Corporation
Aerodynamics Research Department
P. O. Box 235
Buffalo, NY 14221

Professor R. F. Probstein
Department of Mechanical Engineering
Massachusetts Institute of Technology
Cambridge, MA 02139

Commanding Officer
Office of Naval Research Branch Office
536 South Clark Street
Chicago, IL 60605

Code 753
Naval Weapons Center
China Lake, CA 93555

Mr. J. Marshall
Code 4063
Naval Weapons Center
China Lake, CA 93555

Professor R. T. Davis
Department of Aerospace Engineering
University of Cincinnati
Cincinnati, OH 45221

Library MS 60-3
NASA Lewis Research Center
21000 Brookpark Road
Cleveland, OH 44135

Dr. J. D. Anderson, Jr.
Chairman, Department of Aerospace
Engineering
College of Engineering
University of Maryland
College Park, MD 20742

Professor W. L. Melnik
Department of Aerospace Engineering
University of Maryland
College Park, MD 20742

Professor O. Burggraf
Department of Aeronautical and
Astronautical Engineering
Ohio State University
1314 Kinnear Road
Columbus, OH 43212

Technical Library
Naval Surface Weapons Center
Dahlgren Laboratory
Dahlgren, VA 22448

Dr. F. Moore
Naval Surface Weapons Center
Dahlgren Laboratory
Dahlgren, VA 22448

Technical Library 2-51131
LTV Aerospace Corporation
P. O. Box 5907
Dallas, TX 75222

Library, United Aircraft Corporation
Research Laboratories
Silver Lane
East Hartford, CT 06108

Technical Library
AVCO-Everett Research Laboratory
2385 Revere Beach Parkway
Everett, MA 02149

Professor G. Moretti
Polytechnic Institute of New York
Long Island Center
Department of Aerospace Engineering
and Applied Mechanics
Route 110
Farmingdale, NY 11735

Professor S. G. Rubin
Polytechnic Institute of New York
Long Island Center
Department of Aerospace Engineering
and Applied Mechanics
Route 110
Farmingdale, NY 11735

Dr. W. R. Briley
Scientific Research Associates, Inc.
P. O. Box 498
Glastonbury, CT 06033

Professor P. Gordon
Calumet Campus
Department of Mathematics
Purdue University
Hammond, IN 46323

Library (MS 185)
NASA Langley Research Center
Langley Station
Hampton, VA 23665

Professor A. Chapmann
Chairman, Mechanical Engineering
Department
William M. Rice Institute
Box 1892
Houston, TX 77001

Technical Library
Naval Ordnance Station
Indian Head, MD 20640

Professor D. A. Caughey
Sibley School of Mechanical and
Aerospace Engineering
Cornell University
Ithaca, NY 14850

Professor E. L. Resler
Sibley School of Mechanical and
Aerospace Engineering
Cornell University
Ithaca, NY 14850

Professor S. F. Shen
Sibley School of Mechanical and
Aerospace Engineering
Ithaca, NY 14850

Library
Midwest Research Institute
425 Volker Boulevard
Kansas City, MO 64110

Dr. M. M. Hafez
Flow Research, Inc.
P. O. Box 5040
Kent, WA 98031

Dr. E. M. Murman
Flow Research, Inc.
P. O. Box 5040
Kent, WA 98031

Dr. S. A. Orszag
Cambridge Hydrodynamics, Inc.
54 Baskin Road
Lexington, MA 02173

Dr. P. Bradshaw
Imperial College of Science and
Technology
Department of Aeronautics
Prince Consort Road
London SW7 2BY, England

Professor T. Cebeci
California State University,
LongBeach
Mechanical Engineering Department
Long Beach, CA 90840

Mr. J. L. Hess
Douglas Aircraft Company
3855 Lakewood Boulevard
Long Beach, CA 90808

Dr. H. K. Cheng
University of Southern California,
University Park
Department of Aerospace Engineering
Los Angeles, CA 90007

Professor J. D. Cole
Mechanics and Structures Department
School of Engineering and Applied
Science
University of California
Los Angeles, CA 90024

Engineering Library
University of Southern California
Box 77929
Los Angeles, CA 90007

Dr. C. -M. Ho
Department of Aerospace Engineering
University of Southern California,
University Park
Los Angeles, CA 90007

Dr. T. D. Taylor
The Aerospace Corporation
P. O. Box 92957
Los Angeles, CA 90009

Commanding Officer
Naval Ordnance Station
Louisville, KY 40214

Mr. B. H. Little, Jr.
Lockheed-Georgia Company
Department 72-74, Zone 369
Marietta, GA 30061

Professor E. R. G. Eckert
University of Minnesota
241 Mechanical Engineering Building
Minneapolis, MN 55455

Library
Naval Postgraduate School
Monterey, CA 93940

Supersonic-Gas Dynamics Research
Laboratory
Department of Mechanical Engineering
McGill University
Montreal 12, Quebec, Canada

Dr. S. S. Stahara
Nielsen Engineering & Research, Inc.
510Clyde Avenue
Mountain View, CA 94043

Engineering Societies Library
345 East 47th Street
New York, NY 10017

Professor A. Jameson
New York University
Courant Institute of Mathematical
Sciences
251 Mercer Street
New York, NY 10012

Professor G. Miller
Department of Applied Science
New York University
26-36 Stuyvesant Street
New York, NY 10003

Office of Naval Research
New York Area Office
715 Broadway - 5th Floor
New York, NY 10003

Dr. A. Vaglio-Laurin
Department of Applied Science
26-36 Stuyvesant Street
New York University
New York, NY 10003

Professor H. E. Rauch
Ph.D. Program in Mathematics
The Graduate School and University
Center of the City University of
New York
33 West 42nd Street
New York, NY 10036

Librarian, Aeronautical Library
National Research Council
Montreal Road
Ottawa 7, Canada

Lockheed Missiles and Space Company
Technical Information Center
3251 Hanover Street
Palo Alto, CA 94304

Commanding Officer
Office of Naval Research Branch Office
1030 East Green Street
Pasadena, CA 91106

California Institute of Technology
Engineering Division
Pasadena, CA 91109

Library
Jet Propulsion Laboratory
4800 Oak Grove Drive
Pasadena, CA 91103

Professor H. Liepmann
Department of Aeronautics
California Institute of Technology
Pasadena, CA 91109

Mr. L. I. Chasen, MGR-MSD Lib.
General Electric Company
Missile and Space Division
P. O. Box 8555
Philadelphia, PA 19101

Mr. P. Dodge
Airesearch Manufacturing Company
of Arizona
Division of Garrett Corporation
402 South 36th Street
Phoenix, AZ 85010

Technical Library
Naval Missile Center
Point Mugu, CA 93042

Professor S. Bogdonoff
Gas Dynamics Laboratory
Department of Aerospace and
Mechanical Sciences
Princeton University
Princeton, NJ 08540

Professor S. I. Cheng
Department of Aerospace and
Mechanical Sciences
Princeton University
Princeton, NJ 08540

Dr. J. E. Yates
Aeronautical Research Associates
of Princeton, Inc.
50 Washington Road
Princeton, NJ 08540

Professor L. Sirovich
Division of Applied Mathematics
Brown University
Providence, RI 02912

Dr. P. K. Dai (RI/2178)
TRW Systems Group, Inc.
One Space Park
Redondo Beach, CA 90278

Redstone Scientific Information Center
Chief, Document Section
Army Missile Command
Redstone Arsenal, AL 35809

U.S. Army Research Office
P. O. Box 12211
Research Triangle, NC 27709

Editor, Applied Mechanics Review
Southwest Research Institute
8500 Culebra Road
San Antonio, TX 78228

Library and Information Services
General Dynamics-CONVAIR
P. O. Box 1128
San Diego, CA 92112

Dr. R. Magnus
General Dynamics-CONVAIR
Kearny Mesa Plant
P. O. Box 80847
San Diego, CA 92138

Mr. T. Brundage
Defense Advanced Research Projects
Agency
Research and Development Field Unit
APO 146, Box 271
San Francisco, CA 96246

Office of Naval Research
San Francisco Area Office
One Hallidie Plaza, Suite 601
San Francisco, CA 94102

Library
The RAND Corporation
1700 Main Street
Santa Monica, CA 90401

Dr. P. E. Rubbert
Boeing Aerospace Company
Boeing Military Airplane Development
Organization
P. O. Box 3707
Seattle, WA 98124

Dr. H. Yoshihara
Boeing Aerospace Company
P. O. Box3999
Mail Stop 41-18
Seattle, WA 98124

Mr. R. Feldhuhn
Naval Surface Weapons Center
White Oak Laboratory
Silver Spring, MD 20910

Librarian
Naval Surface Weapons Center
White Oak Laboratory
Silver Spring, MD 20910

Dr. J. M. Solomon
Naval Surface Weapons Center
White Oak Laboratory
Silver Spring, MD 20910

Professor J. H. Ferziger
Department of Mechanical Engineering
Stanford University
Stanford, CA 94305

Professor K. Karamcheti
Department of Aeronautics and
Astronautics
Stanford University
Stanford, CA 94305

Professor M. van Dyke
Department of Aeronautics and
Astronautics
Stanford University
Stanford, CA 94305

Professor O. Bunemann
Institute for Plasma Research
Stanford University
Stanford, CA 94305

Engineering Library
McDonnell Douglas Corporation
Department 218, Building 101
P. O. Box 516
St. Louis, MO 63166

Dr. R. J. Hakkinen
McDonnell Douglas Corporation
Department 222
P. O. Box 516
St. Louis, MO 63166

Dr. R. P. Heinisch
Honeywell, Inc.
Systems and Research Division -
Aerospace Defense Group
2345 Walnut Street
St. Paul, MN 55113

Dr. N. Malmuth
Rockwell International Science Center
1049 Camino Dos Rios
P. O. Box 1085
Thousand Oaks, CA 91360

Library
Institute of Aerospace Studies
University of Toronto
Toronto 5, Canada

Professor W. R. Sears
Aerospace and Mechanical Engineering
University of Arizona
Tucson, AZ 85721

Professor A. R. Seebass
Department of Aerospace and Mechanical
Engineering
University of Arizona
Tucson, AZ 85721

Dr. K. T. Yen
Code 3015
Naval Air Development Center
Warminster, PA 18974

Air Force Office of Scientific Research
(SREM)
Building 1410, Bolling AFB
Washington, DC 20332

Chief of Research and Development
Office of Chief of Staff
Department of the Army
Washington, DC 20310

Library of Congress
Science and Technology Division
Washington, DC 20540

Director of Research (Code RR)
National Aeronautics and Space Administration
600 Independence Avenue, SW
Washington, DC 20546

Library
National Bureau of Standards ✓
Washington, DC 20234

National Science Foundation
Engineering Division
1800 G Street, NW
Washington, DC 20550

Mr. W. Koven
AIR 03E
Naval Air Systems Command
Washington, DC 20361

Mr. R. Siewert
AIR 320D
Naval Air Systems Command
Washington, DC 20361

Technical Library Division
AIR 604
Naval Air Systems Command
Washington, DC 20361

Code 2627
Naval Research Laboratory ✓
Washington, DC 20375

SEA 03512
Naval Sea Systems Command ✓
Washington, DC 20362

SEA 09G3
Naval Sea Systems Command ✓
Washington, DC 20362

Dr. A. L. Slafkosky
Scientific Advisor
Commandant of the Marine Corps (Code AX)
Washington, DC 20380

Director
Weapons Systems Evaluation Group
Washington, DC 20305

Chief of Aerodynamics
AVCO Corporation
Missile Systems Division
201 Lowell Street
Wilmington, MA 01887

Research Library
AVCO Corporation
Missile Systems Division
201 Lowell Street
Wilmington, MA 01887

AFAPL (APRC)
AB
Wright Patterson, AFB, OH 45433

Dr. Donald J. Harney
AFFDL/FX
Wright Patterson AFB, OH 45433